Research Paper

Impaired telomere pathway and fertility in Senescence-Accelerated Mice Prone 8 females with reproductive senescence

Alba M. Polonio[1], Marta Medrano[1], Lucía Chico-Sordo[1], Isabel Córdova-Oriz[1], Mauro Cozzolino[2], José Montans[3], Sonia Herraiz[1], Emre Seli[4,5], Antonio Pellicer[2,6], Juan A. García-Velasco[1,7,8], Elisa Varela[1,8]

[1]IVI Foundation, The Health Research Institute La Fe (IIS La Fe), Valencia, Spain
[2]IVIRMA Rome, Rome, Italy
[3]Centro Anatomopatológico, Madrid, Spain
[4]IVIRMA New Jersey, Basking Ridge, NJ 07920, USA
[5]Department of Obstetrics, Gynecology and Reproductive Sciences, Yale School of Medicine, New Heaven, CT 06510, USA
[6]Department of Pediatrics, Obstetrics and Gynecology, University of Valencia, Valencia, Spain
[7]IVIRMA Madrid, Madrid, Spain
[8]Department of Obstetrics and Gynecology, Rey Juan Carlos University, Madrid, Spain

Correspondence to: Elisa Varela; **email:** Mariaelisa.Varela@ivirma.com, https://orcid.org/0000-0002-5361-3877
Keywords: telomere, telomerase, aging, fertility, ovary, SAMP8
Received: December 16, 2022 **Accepted:** May 4, 2023 **Published:** May 23, 2023

ABSTRACT

Ovarian aging is the main cause of infertility and telomere attrition is common to both aging and fertility disorders. Senescence-Accelerated Mouse Prone 8 (SAMP8) model has shortened lifespan and premature infertility, reflecting signs of reproductive senescence described in middle-aged women. Thus, our objective was to study SAMP8 female fertility and the telomere pathway at the point of reproductive senescence. The lifespan of SAMP8 and control mice was monitored. Telomere length (TL) was measured by *in situ* hybridization in blood and ovary. Telomerase activity (TA) was analyzed by telomere-repeat amplification protocol, and telomerase expression, by real-time quantitative PCR in ovaries from 7-month-old SAMP8 and controls. Ovarian follicles at different stages of maturation were evaluated by immunohistochemistry. Reproductive outcomes were analyzed after ovarian stimulation. Unpaired *t*-test or Mann-Whitney test were used to calculate *p*-values, depending on the variable distribution. Long-rank test was used to compare survival curves and Fisher's exact test was used in contingency tables. Median lifespan of SAMP8 females was reduced compared to SAMP8 males ($p = 0.0138$) and control females ($p < 0.0001$). In blood, 7-month-old SAMP8 females presented lower mean TL compared to age-matched controls ($p = 0.041$). Accordingly, the accumulation of short telomeres was higher in 7-month-old SAMP8 females ($p = 0.0202$). Ovarian TA was lower in 7-month-old SAMP8 females compared to controls. Similarly, telomerase expression was lower in the ovaries of 7-month-old SAMP8 females ($p = 0.04$). Globally, mean TL in ovaries and granulosa cells (GCs) were similar. However, the percentage of long telomeres in ovaries ($p = 0.004$) and GCs ($p = 0.004$) from 7-month-old SAMP8 females was lower compared to controls. In early-antral and antral follicles, mean TL of SAMP8 GCs was lower than in age-matched controls ($p = 0.0156$ for early-antral and $p = 0.0037$ for antral follicles). Middle-aged SAMP8 showed similar numbers of follicles than controls, although recovered oocytes after ovarian stimulation were lower ($p = 0.0068$). Fertilization rate in oocytes from SAMP8 was not impaired, but SAMP8 mice produced significantly more

morphologically abnormal embryos than controls (27.03% in SAMP8 vs. 1.22% in controls; $p < 0.001$). Our findings suggest telomere dysfunction in SAMP8 females, at the time of reproductive senescence.

INTRODUCTION

Life expectancy has increased during the last decades [1], but women's reproductive lifespan remains unchanged [2, 3]. This fact has implications both for fertility and elderly health. Firstly, fertility is currently threatened due to socioeconomic factors which motivate couples to delay or even decline parenthood [4], and, secondly, elderly health is compromised, as menopause onset is linked to higher risks of aging-associated diseases [5, 6].

Aging can be defined as the gradual, time-dependent loss of physiological integrity, due to the accumulation of cellular damage which leads to impaired regenerative capacity of tissues and increased susceptibility to disease and death [7]. Telomere attrition has been identified as one of the molecular determinants of aging [7]. Telomeres are nucleoprotein structures composed of a repetitive six-nucleotide (5′TTAGGG3′) DNA sequence, localized at the ends of eukaryotic chromosomes, to prevent chromosome ends from being recognized as DNA breaks and protecting them from DNA repair activities and degradation [8]. However, telomeres shorten during cell divisions because DNA polymerases cannot copy the very ends of chromosomes [9]. The accumulation of critically short telomeres leads to cellular senescence or apoptosis [10, 11], limiting the regenerative capacity of tissues [12]. Telomere shortening is associated with aging [7, 13], and individuals with shorter mean TL than average for their age, have a higher risk of aging-associated diseases [14, 15] and mortality [16]. Telomere shortening can be counteracted by the action of telomerase, a ribonucleoprotein enzyme composed of a reverse transcriptase protein component (*Tert*) and an RNA component (*Terc*), which serves as a template for telomere elongation [17]. In telomerase-deficient mice, the accumulation of short telomeres causes defects in stem cell functionality [18–20] leading to accelerated aging [21, 22] and shortened lifespan [23, 24]. Also, telomerase mutations in humans, result in the so-called telomere syndromes, such as, dyskeratosis congenita [25, 26], aplastic anemia [27], or pulmonary fibrosis [28], showing similar phenotypes to telomerase-deficient mice [15, 19]. In natural conditions, telomerase is detectable in adult and embryonic stem cells, cancer cells and in the germ line [29, 30]. Among ovarian cell types, TA is found in oocytes [31, 32], and granulosa [33, 34] and cumulus cells [35]. Nevertheless, ovaries age at a faster pace compared to other organs [2, 3]. Indeed, ovarian aging is one of the main causes of infertility, characterized by the reduction of both the quantity and the quality of gametes, starting at about mid-thirties and leading to menopause at an average age of 50 years [2–4, 36]. In line with the notion that telomeres are linked to infertility, short telomeres in polar bodies extruded from oocytes are associated with an increased risk of embryo aneuploidy [37]. In addition, decreased TL and low or null TA in GCs and peripheral blood mononuclear cells (PBMCs) are found in women with premature ovarian failure [38–41].

Mouse models resembling the ovarian function decay of middle-aged women are scarce. Among those, Senescence-Accelerated Mice Prone 8 (SAMP8), a spontaneous animal model [42] recapitulates signs of reproductive aging in middle-aged women [43]. The SAMP8 model was generated from the AKR/J strain by selective inbred crosses of mice, based on graded scores for lifespan and senescence, along with pathologic phenotypes [44, 45]. One of the different strains with accelerated senescence, SAMP8 model, displays immune dysfunction [46], altered circadian rhythms [47], behavioral and emotional alterations [48], and memory and learning impairment [44, 48–50], with milder defects in females [49, 51]. SAMP8 has also been proposed as a model of Alzheimer's disease at senectitude [42, 52]. Regarding fertility, the hypothalamus-pituitary-ovary axes is altered in SAMP8 females [53, 54], which, at 7 months of age, have shortened estrous cycles, high levels of FSH, and lower fertility [43]. The concurrence of all these symptoms, which have an early onset compared with SAMP8 lifespan, is similar to middle-aged women's reproductive aging [43].

In addition, SAMP8 has shorter lifespan compared to the control senescence-accelerated mouse resistant 1 (SAMR1) mice [52], which do not have reproductive senescence. Interestingly, several characteristics found in the SAMP8 model are similar to those found in the second and third generation of telomerase-deficient mice, which besides accelerated telomere shortening and reduced lifespan [19, 23, 52] also show spindle aberrations in their oocytes [43, 55], reduced fertility [43, 56], or even fertility loss [19, 43].

In the current study, we sought to investigate whether the SAMP8 mice, which show accelerated-reproductive senescence have alterations in their telomere pathway. This question has not yet been explored in relation to

reproduction in this model. We found alterations in the telomere pathway coinciding with fertility disorders in 7-month-old (29 weeks) female SAMP8 mice, at a time point when the survival was not different compared to controls.

RESULTS

SAMP8 females have shorter lifespan

The lifespan of the SAMP8 mice is shorter than that of the SAMR1 mice [52]. In order to validate the lifespan of SAMP8 and SAMR1 in our housing conditions and to analyze the survival of SAMP8 and SAMR1 females, which has not been shown, we monitored 38 SAMP8 mice and 37 SAMR1 mice under free-intervention conditions. The age of death of mice involved in survival analysis is shown in Supplementary Table 1. Pathologies found after necropsy analysis in the SAMP8 and SAMR1 mice are shown in Supplementary Figures 1 and 2 and described in Supplementary Table 2. SAMP8 presented a 31.05 % shortened median lifespan ($p < 0.0001$) compared to SAMR1 (Table 1 and Figure 1A). Next, we considered males and females separately, to further discern differences in survival distributions of both models. SAMP8 females showed a decreased median lifespan (Table 1 and Figure 1B, left panel) compared to gender-matched controls (60 weeks in SAMP8 vs. 98.14 weeks in SAMR1), reaching a difference of 38.86% ($p < 0.0001$). The ages of death of the upper-longevity quartile were also statistically significantly decreased in SAMP8 compared to SAMR1 females (Figure 1B, right panel; $p = 0.015$). Similarly, SAMP8 males had shorter median lifespan (31.54%; $p < 0.0001$) compared to SAMR1 males (Table 1 and Figure 1C). Comparisons of female and male survival (Table 1 and Figure 1D and 1E) showed that in both SAMR1 and SAMP8 models, females presented a shortened median lifespan compared to males (24.18% in SAMP8 model vs. 15.10% in SAMR1 model). Together our results show that SAMP8 females have the shortest median and maximum survival among the different groups analyzed.

Telomere maintenance is altered in 7-month-old SAMP8 females

Because SAMP8 mice had a survival curve enclosed between the curves of telomerase-deficient mice of the second and third generation [23] we next analyzed TL in PBMCs (Figure 2A). TL analysis (Figure 2B and 2C) showed that, at 7 months of age, SAMP8 females presented a statistically significant decrease in mean TL compared to age-matched controls (281.1 a.u. in SAMP8 vs. 359 a.u. in SAMR1, $p = 0.041$). Of note, no differences in mean TL were found between 3-month-old SAMP8 females and age-matched SAMR1 (Supplementary Figure 3A and 3B), or 3- or 7- month-old SAMP8 males and their age-matched controls (Supplementary Figure 3C–3F). Critically short telomeres are important because they limit cell division, leading to tissue regeneration impairment and shorter lifespan [10]. Comparing the accumulation of critically short telomeres (10^{th} percentile) in PBMCs [57], we found that 7-month-old SAMP8 females presented a statistically significantly higher percentage of critically short telomeres (Figure 2D) than age-matched SAMR1 females (32.03% in SAMP8 vs. 13.21% in SAMR1; $p = 0.0202$). In line with this result, the mean percentage of long telomeres (90^{th} percentile) was lower in 7-month-old SAMP8 females (6.128% in SAMP8 vs. 12.18% in SAMR1, $p = 0.0511$) although it did not reach statistical significance (Figure 2E). Interestingly, these differences in TL did not correspond to differences in the probability of survival (100% in SAMP8 in 94.74% in SAMR1; p value > 0.999) of SAMP8 and SAMR1 females, at the age of 7 months (Figure 2F). Together our results suggest that the telomere pathway is altered in females of the SAMP8 mouse model at an age of 7 months, when survival is similar for both models.

Ovarian telomeres are altered in 7-month-old SAMP8 females

SAMP8 females have reproductive senescence at the age of 7 months [43], coinciding with systemic alterations in blood TL. Several lines of evidence point to an association between telomere alterations and fertility disorders [34, 55, 56]. Thus, we investigated telomere pathway in the ovary. We first explored TA by TRAP assay and found lower levels in SAMP8 females at the age of 7 months (Figure 2G and 2H) compared to age-matched SAMR1 and young females. Comparing both models at the age of 7 months, 73.33% of SAMP8 females showed lower TA levels in ovarian samples ($n = 15$). We then measured the levels of *Tert* expression, which correlate with TA [58]. In the ovaries of 7-month-old SAMP8 females, *Tert* expression was statistically significantly lower compared to SAMR1 females (0.543 in SAMP8 vs. 1.348 in SAMR1, $p = 0.040$) (Figure 3A). In order to determine if lower *Tert* expression would have an impact on telomere maintenance, TL in ovaries was measured (Figure 3B). Statistically significant differences were not found in mean TL either globally or in GCs (Supplementary Figure 4, Table 2). However, 7-month-old SAMP8 females presented a statistically significantly lower percentage of long telomeres (Figure 3C, Table 2) in both global ovarian tissue (6.65 in SAMP8 vs. 11.11% in SAMR1, $p = 0.04$) and GCs (6.23% in SAMP8 vs. 11.92% in SAMR1, $p = 0.04$). Although higher percentages of short telomeres were systematically

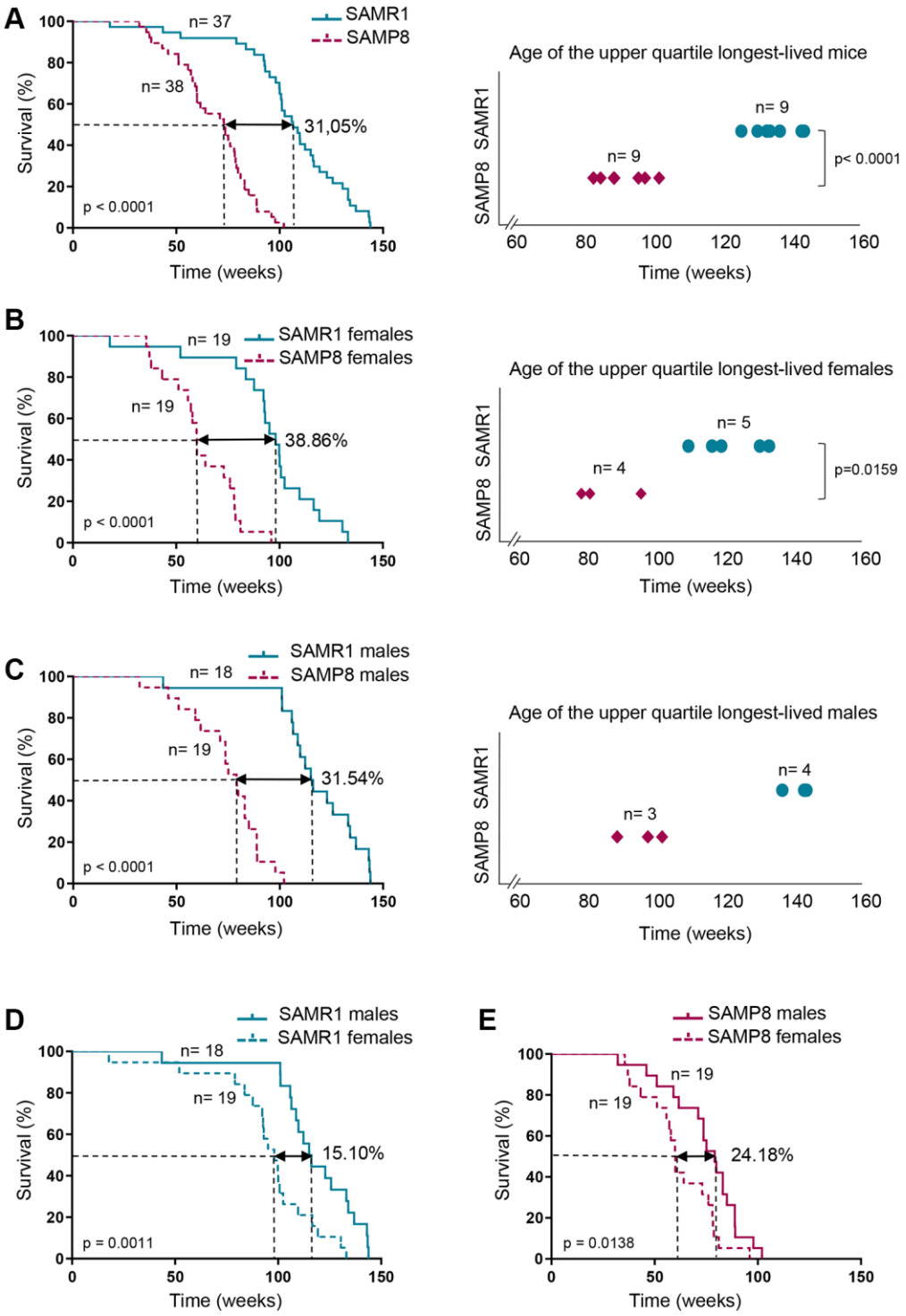

Figure 1. Analysis of SAMP8 and SAMR1 lifespan. (**A**) Kaplan-Meier plot of survival of SAMP8 (purple lines) and SAMR1 (turquoise lines) in the left panel, and graphic representation of the time of death of the Q3 longest-lived SAMP8 (purple rhombus) and SAMR1 (turquoise dots) mice in the right panel. (**B**) Kaplan-Meier plot of survival (left panel) and graphic representation of the time of death of the Q3 longest-lived females (right panel) of the mouse models described in A. (**C**) Kaplan-Meier plot of survival (left panel) and graphic representation of the time of death of the Q3 longest-lived males (right panel) of the mouse models described in A. (**D**) Kaplan-Meier plot of survival of SAMR1 mice breakdown by sex (females in dashed line and males in continued line). (**E**) Kaplan-Meier plot of survival of SAMP8 mice breakdown by sex (females in dashed line and males in continued line). n indicates the number of mice analyzed. Long-rank test was used to calculate *p*-values comparing lifespan distributions (**A**, **B** and **C**, left panels; **D** and **E**). *t*-test was used to determine *p*-value when comparing maximum lifespan of the upper quartile longest-lived mice (**A**, right panel). Mann-Whitney *U* test was used to determine *p*-value in maximum lifespan of the upper quartile longest-lived mice (**B** and **C**, right panels).

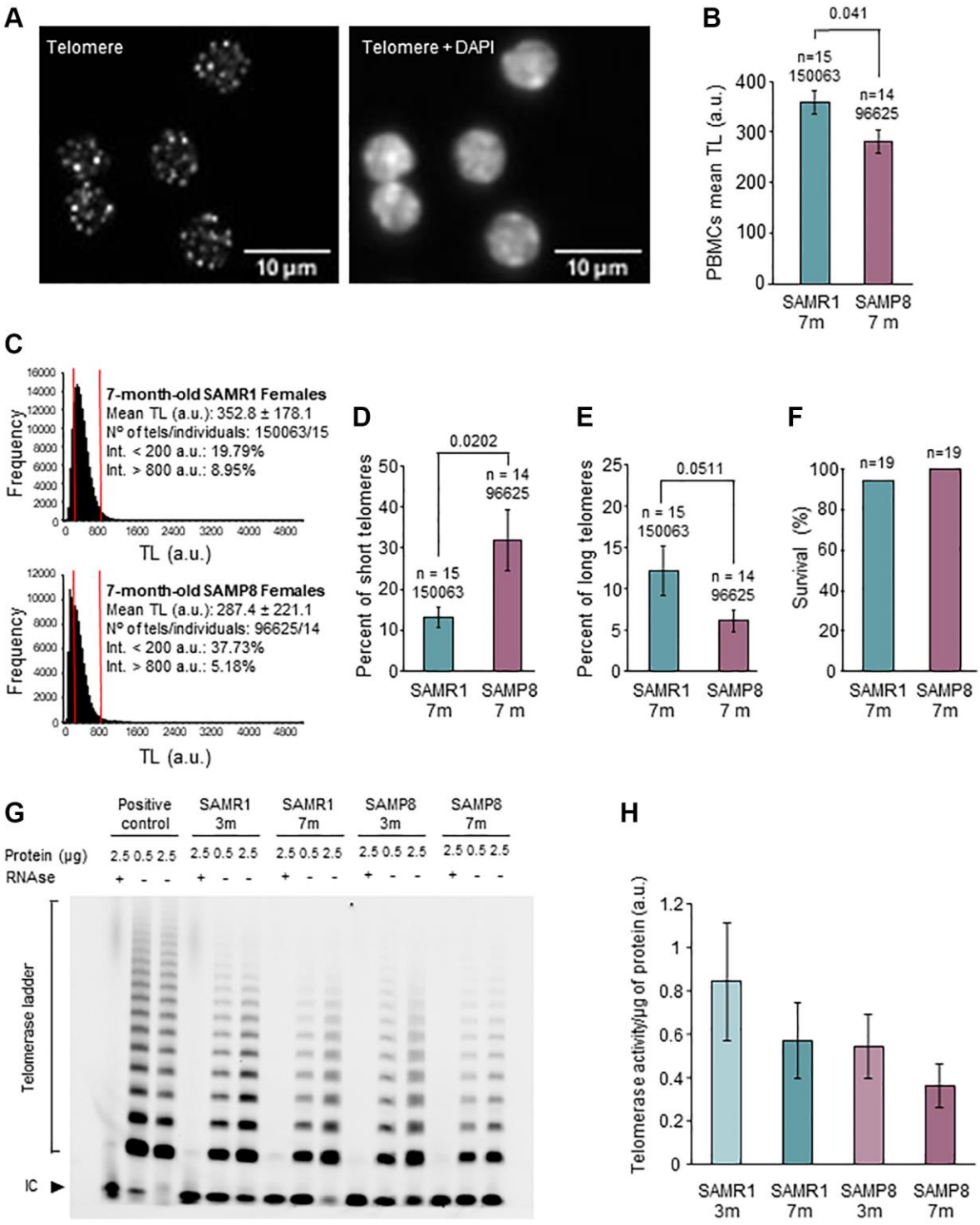

Figure 2. Analysis of telomere length in PBMCs and telomerase activity in ovary. (**A**) The micrographs show representative images of telomere HT-qFISH (white dots, left panel) and the merge (DAPI and telomeres, right panel) on PBMCs. (**B**) Mean TL of PBMCs, analyzed by HT-qFISH, in 7-month-old SAMP8 and SAMR1 females. (**C**) Telomere-length frequency histograms in 7-month-old controls (top panel) and age-matched SAMP8 females (lower panel). (**D**) Percent of short telomeres in PBMCs of 7-month-old SAMP8 and SAMR1 females. (**E**) Percent of long telomeres in PBMCs of 7-month-old SAMP8 and SAMR1 females. (**F**) The graph shows the percent of survival at 7 months of age in SAMP8 females and controls. (**G**) The micrograph shows telomerase activity assay from ovarian extracts of SAMP8 and SAMR1 females at 3 and 7 months of age. Two protein concentrations (0.5 and 2.5 µg) of the same ovarian extract from each mouse are shown. (**H**) Quantification of the telomerase activity TRAP assay shown in G. n indicates the number of mice analyzed. Underneath, the number of telomere spots analyzed is indicated. The S.E.M. is represented in error bars (**B**, **D**, **E** and **H**). Statistical significance was determined Mann-Whitney *U* test (**B**, **D** and **E**) and Fisher's exact test (**F**). Abbreviation: IC: Internal Control. Scale bars are 10 µm.

Table 1. Lifespan analysis in SAMP8 and SAMR1 models.

	SAMR1	SAMP8	SAMR1 Females	SAMP8 Females	SAMR1 Males	SAMP8 Males
No of individuals (*n*)	37	38	19	19	18	19
Lifespan (weeks)						
Median	106.4	73.36	98.14	60.0	115.6	79.14
(95% CI)	(100.0–116.1)	(59.86–78.71)	(87.71–109.7)	(51.14–78.00)	(106.4–134.0)	(61.71–88.86)
Mean ± SD	105.6 ± 27.00	68.44 ± 18.33	94.93 ± 26.23	62.14 ± 16.86	116.8 ± 23.56	74.75 ± 17.95
p-value	–	<0.0001[1]	–	<0.0001[1]	–	<0.0001[1]
p-value	–	–	(0.0009)[1]	(0.0319)[2]	–	–
Maximum survival (weeks)						
Age at death	143.9	102.0	133.1	96.0	143.9	102.0

p-value was calculated between SAMP8 and SAMR1 groups (globally, females and males). Brackets indicate *p*-value calculated between females and males of the same model. [1]*p*-value was calculated using Mann-Whitney *U* test (groups with non-normal distribution of data). [2]*p*-value was calculated using Student *t*-test (groups with normal distribution of data).

found in SAMP8 samples, they did not reach statistical significance (Table 2). Given that GCs intensely proliferate during folliculogenesis, we analyzed separately GCs from each follicular stage (Figure 3D). Mean TL of GCs in primordial, primary and secondary follicles, was not different in SAMP8 and SAMR1 ovaries (Figure 3E, Table 2). Interestingly, mean TL was statistically significantly decreased in 7-month-old SAMP8 females in GCs from early-antral (100.8 a.u. in SAMP8 vs. 114.0 a.u. in SAMR1, $p = 0.0159$) and antral follicles (105.9 a.u. in SAMP8 vs. 116.7 a.u. in SAMR1, $p = 0.0037$) compared to age-matched controls (Figure 3F, Table 2). In SAMP8 females (Figure 3G, Table 2), lower accumulation of long telomeres was found in early-antral (3.03% in SAMP8 vs. 13.66% in SAMR1, $p = 0.0159$) and antral follicles (3.36% in SAMP8 vs. 10.73% in SAMR1, $p = 0.0025$). An increased percentage of critically short telomeres (Table 2) was also found in antral follicles of SAMP8 females (28.78% in SAMP8 vs. 11.31% in SAMR1, $p = 0.0225$). Our results suggest that lower *Tert* expression levels and TA may impact TL of GCs in developing follicles.

Ovarian function is altered in 7-month-old SAMP8 females

In telomerase-deficient mice organ function is impaired [19]. Since SAMP8 had lower TA and *Tert* levels in the ovary and lower mean TL in early-antral follicles, we tested ovarian function. Ovarian weight normalized by body mass of SAMP8 females was higher than controls (Figure 4A; $p = 0.017$), accompanied by the presence of numerous corpus luteum, found in histopathological analysis (Supplementary Figure 5). Despite the higher ovarian weight, there were not differences in absolute numbers of either total follicles or in the different follicular stages (Figure 4B and 4C). Mean number of primary follicles was higher in SAMP8 females (59.31%), although it did not reach statistical significance (Figure 4C). This was also observed when follicular stages were represented as percentages (34.77% in SAMP8 vs. 20.26% in SAMR1; $p = 0.0567$) (Figure 4D). Premature ovarian aging is reflected in the gamete production and fertility [3]. Therefore, we analyzed the number of oocytes collected (Figure 4E) after ovarian stimulation (OS), finding that 7-month-old SAMP8 females produced significantly lower number of oocytes ($p = 0.0068$). Fertilization rate was not impaired in SAMP8 females (Figure 4F) and the number of collected embryos were not different between the groups (Figure 4G). However, the percentage of morphologically abnormal embryos was significantly higher in SAMP8 females (27.03% in SAMP8 vs. 1.22% in SAMR1; $p < 0.001$; Figure 4H and 4I). Our results suggest that oogenesis and embryo development is impaired in 7-month-old SAMP8 mice compared to age-matched controls, coinciding with alterations in the telomere pathway.

DISCUSSION

In this work, we have found, a robust phenotype, in terms of reduced lifespan, in SAMP8 females. Interestingly, at the age of 7 months, when survival was similar in both groups, TL in PBMCs was shorter and TA was decreased in SAMP8 females compared to age-matched SAMR1 female mice. In addition, in the middle-aged (7-month-old) SAMP8 females, TA, telomerase expression and the accumulation of longer telomeres in the ovaries were reduced. These changes coincided with impaired reproductive function in SAMP8 mice, with decreased number of collected oocytes after OS and higher percentage of morphologically abnormal embryos.

Regarding lifespan, the median and maximum values obtained for SAMP8 were lower than in SAMR1, as

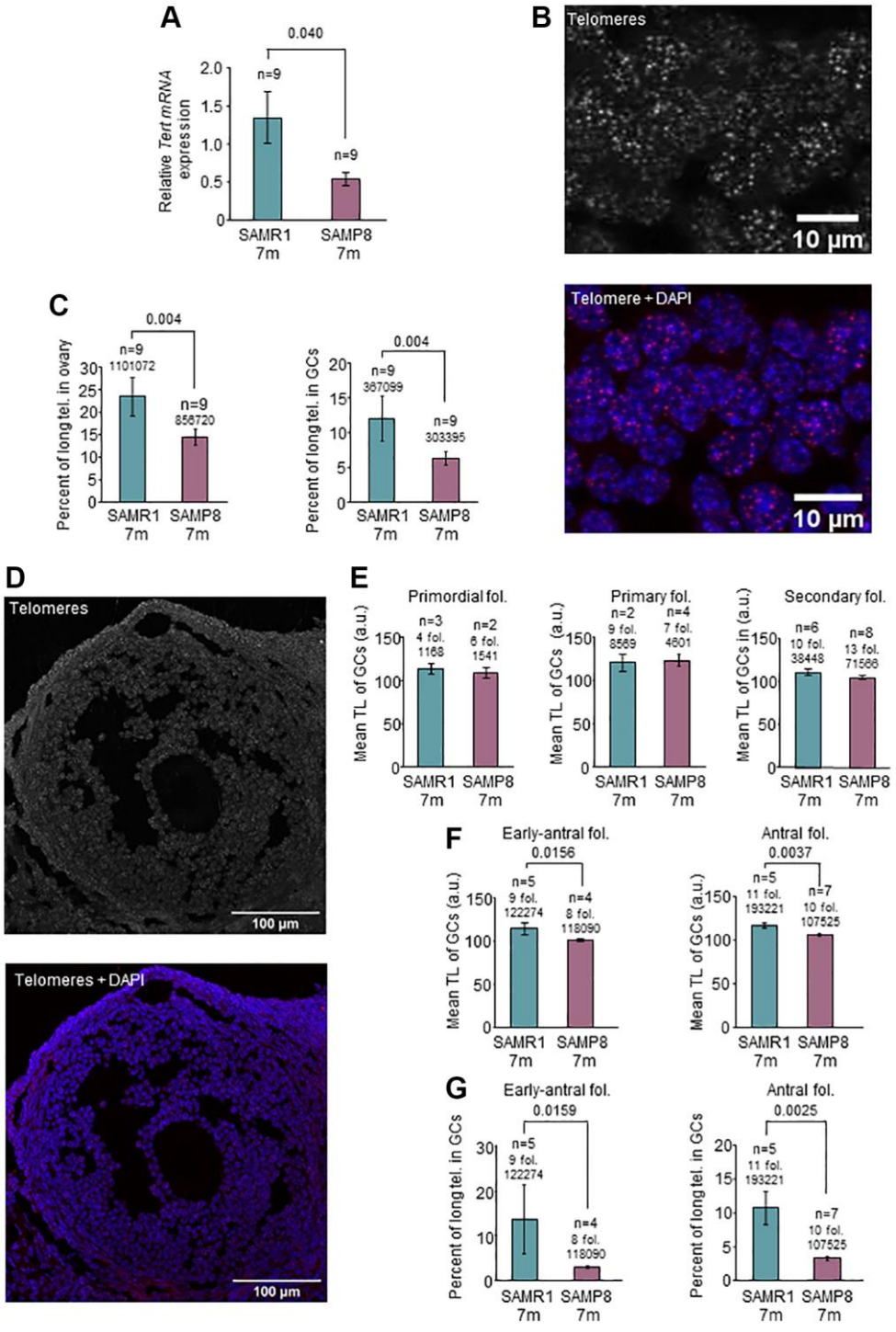

Figure 3. Analysis of *Tert* expression and telomere length in the ovary. (**A**) The graph shows mean mRNA expression of *Tert* normalized by *Gapdh* in the ovary of 7-month-old SAMP8 and SAMR1 females, measured by RT-qPCR. (**B**) The micrographs show representative images of telomere FISH on ovarian sections (white dots, left panel) and the merge (DAPI in blue and telomeres in red, right panel). (**C**) Percent of long telomeres in the ovary (left panel) and in GCs (right panel) in 7-month-old SAMP8 and SAMR1 females. (**D**) The micrographs show representative images of an antral follicle after telomere FISH (white dots, top panel) and the merge (DAPI in blue and telomeres in red, lower panel). (**E**) Mean TL, analyzed by FISH, of GCs of primordial, primary and secondary follicles in 7-month-old SAMP8 and SAMR1 females. (**F**) Mean TL, analyzed by FISH, of GCs of early-antral (left panel) and antral (right panel) follicles in 7-month-old SAMP8 and SAMR1 females. (**G**) Percent of long telomeres in GCs of early-antral (left panel) and antral follicles (right panel) in 7-month-old SAMP8 and SAMR1 females. n indicates the number of mice analyzed. Underneath the n or the number of follicles, the number of telomere spots is indicated. The S.E.M. is represented in error bars (**A**, **C**, **E**, **F** and **G**). Statistical significance was determined by unpaired *t*-test (**E** and **F**, right panels) and Mann-Whitney *U* test, for the rest of graphs. Scale bars are 10 µm (**B**) and 100 µm (**D**).

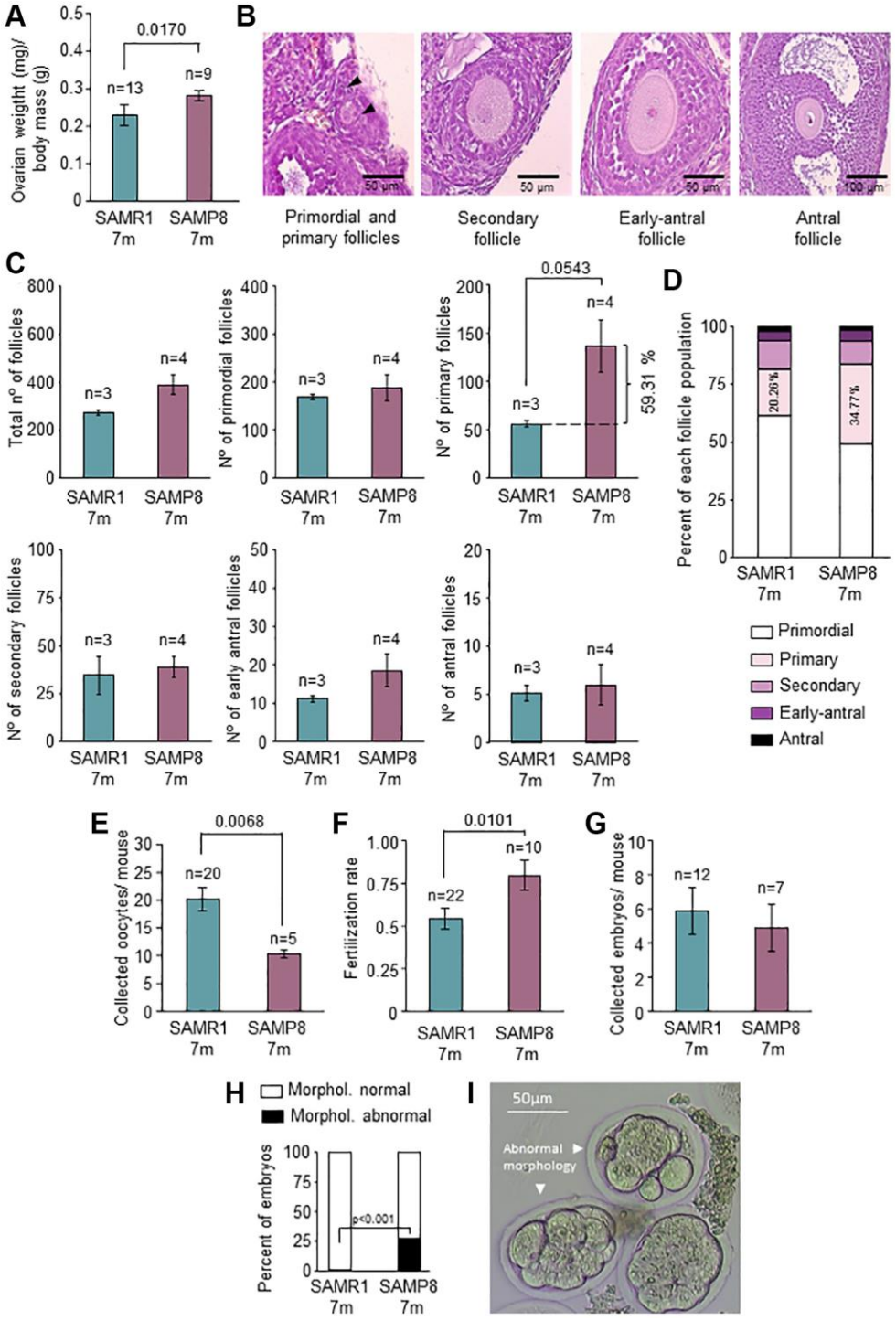

Figure 4. Characterization of ovarian function and fertility. (**A**) The graph shows the ratio of ovarian weight normalized to total body mass in 7-month-old SAMP8 and SAMR1 females. (**B**) Representative images of primordial, primary, secondary, early-antral, and antral follicles in H&E-stained ovarian sections. (**C**) Follicle count in H&E-stained ovarian sections in the mice described in A. The total number of follicles (left top panel), primordial (middle top panel), primary (right top panel), secondary (left lower panel), early-antral (middle lower panel) and antral follicles (right lower panel) are represented. (**D**) The graph shows follicle types in percentages in mice described in A. The percentages of primary follicles are indicated inside the corresponding box. (**E**) Mean number of collected oocytes after OS in mice described in A. (**F**) Fertilization rate in mice described in A. (**G**) Mean number of collected embryos after ovarian stimulation in mice described in A. (**H**) Percent of morphologically normal and abnormal embryos in mice described in A. (**I**) Representative images of preimplantation embryos (morphologically abnormal embryos are indicated with arrows). n indicates the number of mice analyzed. The S.E.M. is represented in error bars (**A**, **C**, **E**, **F** and **G**). Statistical significance was determined by Mann-Whitney *U* test (**A**, **C**, **E** and **F**) and unpaired *t*-test (**G**). Fisher's exact test was used to determine *p*-values (**H**). Scale bars are 50 µm (**B**, left and middle panel) and 100 µm (**B**, right panel).

Table 2. Telomere analysis in ovaries from 7-months old SAMP8 and SAMR1 females.

	TL		Percent of short telomeres		Percent of long telomeres	
	Mean ± SD		Mean ± SD		Mean ± SD	
	SAMR1	SAMP8	SAMR1	SAMP8	SAMR1	SAMP8
Global ovarian tissue	111.6 ± 8.097	106.4 ± 3.493	12.46 ± 6.584	16.06 ± 5.957	11.11 ± 7.417	6.649 ± 1.885
Number of individuals	9	9	9	9	9	9
p-value	0.0625[1]		0.2419[2]		0.0400[1]	
GCs	110.4 ± 10.40	105.0 ± 4.878	13.19 ± 10.50	15.30 ± 7.068	11.92 ± 9.690	6.226 ± 2.842
Number of individuals	9	9	9	9	9	9
p-value	0.1785[2]		0.3401[1]		0.0400[1]	
GCs in primordial follicles	113.5 ± 9.976	108.9 ± 8.627	11.76 ± 10.94	25.72 ± 15.12	11.0 ± 9.039	10.01 ± 6.474
Number of follicles	4	6	4	6	4	6
p-value	0.800[1]		0.400[1]		>0.9999[1]	
GCs in primary follicles	120.3 ± 13.22	123.1 ± 14.36	15.00 ± 17.82	28.82 ± 13.22	13.08 ± 12.21	4.378 ± 2.504
Number of follicles	9	7	9	7	9	7
p-value	>0.999[1]		0.2571[1]		0.1194[2]	
GCs in secondary follicles	110.4 ± 9.248	104.3 ± 6.679	12.21± 7.681	16.70 ± 9.482	11.09 ± 8.175	6.151 ± 3.993
Number of follicles	10	13	10	13	10	13
p-value	0.1743[2]		0.3627[2]		0.3450[1]	
GCs in early-antral follicles	114.0 ± 15.38	100.8 ± 2.421	25.66 ± 26.92	29.82 ± 5.625	13.66 ± 17.07	3.032 ± 0.7869
Number of follicles	9	8	9	8	9	8
p-value	0.0159[1]		0.7731[2]		0.0159[1]	
GCs in antral follicles	116.7 ± 6.858	105.9 ± 2.970	11.31 ± 6.418	28.78 ± 13.30	10.73 ± 5.438	3.362 ± 0.8148
Number of follicles	11	10	11	10	11	10
p-value	0.0037[2]		0.0225[2]		0.0025[1]	

[1]*p*-value was calculated using Mann-Whitney *U* test (groups with non-normal distribution of data). [2]*p*-value was calculated using Student *t*-test (groups with normal distribution of data).

shown earlier [52]. Female mice of both models had a lower median survival compared to males, and SAMP8 females presented the shortest median and maximum lifespan of the mice studied. Our postmortem-examination findings coincide with former reports for both models [59, 60]. Interestingly, the survival curve of SAMP8 mice resembled that of telomerase-deficient mice, lying between the ones of second- and third-generations without telomerase [23], in whose absence, telomere shortening is increased on each subsequent generation [24].

Concerning telomeres, which are a primary cause of aging [7], TL was shorter in PBMCs of middle-aged SAMP8 females. Moreover, SAMP8 females accumulated more critically short telomeres, which are shown to correlate with lifespan [10]. Indeed, critically short telomeres may cause cellular senescence [7], and the accumulation of senescence cells in tissues leads to aging [61, 62]. Ultimately, TA is responsible for TL maintenance [63]. In fact, in humans, lower TA levels lead to telomere shortening and the development of severe diseases such as liver cirrhosis [64], pulmonary fibrosis [28], aplastic anemia [27] and dyskeratosis congenita [65]. These disorders concur with shorter lifespan and limited regenerative capacity of tissues [14, 15].

An association between telomeres and fertility has been evidenced in mice [19, 23, 34, 55, 56] and in women with fertility disorders, in whom TL and TA alterations have been described [33, 35, 38–41, 66]. Recently, in a case of dyskeratosis congenita, with altered TA, diminished fertility has been reported [66], with decreased oocyte production and fertilization rate, along with increased rate of aneuploidy and shorter TL in embryos [66]. Here, in SAMP8 females, with accelerated reproductive senescence [43] we observed lower TA and telomerase expression in ovaries, which are determinants of fertility outcomes [33]. Indeed, telomerase-deficient mice produce a lower number of oocytes, which have spindle abnormalities and chromosome misalignments [56]. Most embryos from telomerase-deficient mice do not reach the blastocyst stage, leading to reduced litter size [19]. The SAMP8 model also shows reduced littler size [43] and oocytes

with spindle aberrations and chromosome mis-alignments [43].

Correct oocyte maturation needs an adequate ovarian niche. In 7-month-old SAMP8 females, ovarian weight was higher than in wild types, although the numbers of follicles were similar. The accumulation of corpus luteum in this model could be a plausible explanation, and also suggests a potential impairment of the pathways involved in corpus luteum regression [67, 68]. Unprecedently, we found a trend to the accumulation of primary follicles in SAMP8 females. This points to either more primordial follicles being recruited for follicular development or primary follicles having limitations to advance toward secondary follicles. Later in folliculogenesis, the number of antral follicles was similar in both models, however, the number of collected oocytes after OS was lower in the SAMP8 model, as previously shown [43]. Despite the straightforward fertilization competence of the 7-month-old SAMP8 oocytes, there was a trend to a lower production of embryos in SAMP8 females. Indeed, a remarkably high number of alterations in the morphology of preimplantation embryos in SAMP8 females was scored. This suggests that follicular development in the SAMP8 mice might yield mature oocytes but the molecular mechanisms that prevent aneuploidies may not function accurately. These results resemble what occurs in middle-aged women in whom not only the quantity of gametes is diminished [3], but also a higher rate of aneuploidies is found [69], particularly when TL is low in polar bodies extruded from oocytes [37].

In the context of the ovary, unexpectedly TL was similar in SAMP8 and SAMR1 mice, despite the lower TA and *Tert* expression in middle-aged SAMP8 females. However, globally, both in the ovary and GCs, the accumulation of long telomeres was lower in the SAMP8, which could be explained by the preferential action of telomerase on short telomeres [70]. In wild types, telomeres of GCs may be protected from excessive shortening [17] because of the presence of TA [31–34, 71]. In SAMP8 females, even reduced telomerase levels could still maintain telomeres at early follicular stages (primordial and primary follicles, which we found to have similar TL as controls) because cell division is limited. To reach later stages of folliculogenesis, GCs have to undergo active and repetitive cell divisions [72], and reduced telomerase may not be able to sustain wild-type levels of TL. This could explain the lower mean TL and percentage of long telomeres found in early-antral and antral follicles as well as the increment in the percentage of critically short telomeres found in antral follicles of SAMP8 mice. Thus, lower levels of telomerase in the ovary seem to impact telomere maintenance of GCs at the end of follicle development.

Overall, our results suggest that the telomere pathway is altered in middle-aged SAMP8 females not only at the systemic level (shorter telomeres in PBMCs) but also in the ovarian compartment (lower telomerase expression and activity as well as altered telomeres in GCs). All of it concurs with the onset of reproductive senesce symptoms in the SAMP8, at a time in which survival is not altered. Dysfunctions in the telomere pathway are also observed in women with fertility disorders [38, 40, 66]. In addition, our results show alterations in embryo development, which have also been associated with short telomeres in humans [37].

Understanding the molecular pathways underlying aging and fertility, provides a basis for further studies focused on several topics. First, the analysis of embryo alterations, which can be better assessed in mice than in humans. Second, how reproductive lifespan improvement may ameliorate elderly health. And third, the mechanisms underlying follicle recruitment and development, which are not completely known. Thus, SAMP8 females represent a bona fide model for the analysis of fertility, not only because it shows similar phenotype to middle-aged women as stated earlier [43], but also because the alterations in the telomere pathway are found in women with fertility disorders [37, 38, 40, 41] and this pathway links reproduction with longevity.

METHODS

Animal handling

All animal procedures were performed according to protocols approved by the Ethics Committee of the Rey Juan Carlos University (code 2509201913119) on 18th of November of 2019. The senescence-accelerated mice, selected from inbred crosses of the AKR/J mouse strain [44], were a kind gift of Dr. Helena Mira Aparicio (IBV, CSIC, Valencia, Spain). Mice were raised under specific-pathogen-free conditions and standard 12-h light-dark cycles in Rey Juan Carlos University Animal Production and Experimentation Service and they were provided with food and water *ad libitum*.

Study design

Middle-aged SAMP8 females (7-months old; 29 weeks), with accelerated-reproductive senescence, and age-matched SAMR1 females, which do not have reproductive senescence (controls), were used for experiments.

Survival analysis

SAMR1 mice (n = 37; 19 females and 18 males) and SAMP8 mice (n = 38; 19 females and 19 males) were used for lifespan analysis. All mice were maintained under intervention-free conditions. To determine the time of death, mice were inspected three times per week. Moribund mice were euthanized if they were severely ill or if the veterinarian from the Animal Production and Experimentation Service concluded that they would not survive more than 2 days. The age at which euthanasia was performed was considered as the best estimation of the time of natural death.

Sample collection

Mice were sacrificed by inhalation of carbon dioxide (CO_2) or by cervical dislocation (in the case of oocytes and preimplantation embryos). Ovaries were collected and fat surrounding the ovary was removed, followed by ovarian weight measurement. One ovary was frozen in liquid nitrogen and stored at −80ºC. The other ovary was fixed in 4% formaldehyde for 24 hours and treated as explained below depending on the experiments performed. Blood samples were collected by cardiac puncture in K2-EDTA tubes (BD Vacutainer) and PBMCs were isolated by using Ficoll gradient (Histopaque, Sigma), fixed with methanol: acetic acid (3:1) and stored at 4ºC. In the case of ovaries (Figures 3 and 4), samples were divided for different techniques (FISH, RT-PCR, H&E and TRAP), thus, experiments were done with lower "n" compared to results in Figure 2.

Follicle counts

Fixed ovaries were embedded in paraffin and cut into 4 μm sections. Follicle count was performed on every fifth section stained in Hematoxylin–Eosin (H&E). Follicles were classified as previously described [73] as: (a) primordial: the oocyte was surrounded by a layer of flattened GCs; (b) primary: the oocyte was surrounded by a complete layer of cuboidal GCs; (c) secondary: the oocyte was surrounded by two or more layers of cuboidal GCs; (d) early-antral: the oocyte was surrounded by four or more layers of GCs, forming the follicular atrium; and (e) antral: follicles containing a clearly defined single antral space. To avoid double counting, follicles were only counted when the oocyte nucleus was present in the section. All H&E sections were examined by at least 2 observers.

Real-time quantitative PCR (RT-qPCR)

Ovaries were homogenized using RNAse-free pestle and mortar. Ovarian total RNA isolation was performed using RNAeasy Micro Kit (QIAGEN) following manufacturer's instructions. 1 μg of RNA was retrotranscribed to complementary DNA (cDNA) using iScriptcDNA Synthesis Kit (BioRad) according to manufacturer's recommendations. RT-qPCR was performed using SsoAdvanced Universal SYBR Green Supermix (BioRad) according to manufacturer's protocol in 7500 Fast Real-Time PCR System (Applied BioSystems) by the personnel of the Rey Juan Carlos University Genomics-Flow Cytometry Unit. The primers for the PCR amplification of *Tert* and *Gapdh* (Glyceraldehyde-3-phosphate dehydrogenase) genes are described below. *Gapdh* gene expression was used to calculate the relative expression of *Tert* gene, based on the cycle threshold (Ct).

Gapdh-F 5′-GCACAGTCAAGGCCGAGAAT-3′
Gapdh-R 5′-GCCTTCTCCATGGTGGTGAA-3′
Tert-F 5′-GGATTGCCACTGGCTCCG-3′
Tert-R 5′-TCAATTGGTAAGCTGTAAGTCTGTG-3′.

Telomerase-repeat amplification protocol (TRAP) assay

Ovarian samples were homogenized using RNAse-free pestle and mortar and lysed as in [74]. The CY5-labelled telomerase-substrate primer (TS-primer: 5′-Cy5-AATCCGTCGAGCAGAGTT-3′, Sigma-Aldrich [75]); was elongated, and elongation products were amplified together with an internal control, as in [75]. Two protein concentrations were used for each sample (0.5 and 2.5 μg). A negative control was included by preincubating each sample extract with RNase (Roche Diagnosis) for 10 min at 30°C as in [76]. Jurkat cells were used as a positive control. Electrophoresis was run in an acrylamide: bisacrylamide 19:1 gel (Bio-Rad) using Protean II (Bio-Rad) electrophoresis chambers. Gels with Cy5 signals were imaged wet in ChemiDoc (Bio-Rad). Image Lab software (version 5.0) was used for quantification of the TRAP image shown in Figure 2.

***In situ* hybridization fluorescence**

TL was assessed in PBMCs and ovaries by fluorescence *in situ* hybridization (FISH). For PBMCs, High-Throughput Quantitative FISH (HT-qFISH) was performed using 96-well plates with clear bottom (Greiner, Bio-One). Fixed cells were attached to plates using poly-L-lysine (Sigma-Aldrich) for 30 min at 37°C and FISH was performed as previously described [57]. Fixed ovaries (see sample collection section) were frozen with OCT and 10 μm sections were cut. FISH on tissue sections was performed as in [76].

Briefly, samples were fixed with 4% formaldehyde for 2 min at room temperature (RT) and permeabilized with Pepsin (Sigma-Aldrich) for 10 min at 37°C. Subsequently, samples were dehydrated with increasing

concentrations of EtOH (70%, 90% and 100% for 5 min at RT, respectively). Tel-Cy3 PNA probe (Cy3-$(CCCTAA)_3$) (Panagene) was added in hybridization solution (containing 70% of deionized formamide) at a final concentration of 0.5 μg/mL. DNA denaturation was performed at 85°C followed by 2 h incubation at RT. Hybridization solution without the probe was added as a negative control. Intensive washes were performed in order to remove non-specifically bound probe. Nuclei were stained with DAPI (Invitrogen) and Vectashield (Vector Laboratories) was added as an antifading agent.

Image acquisition and analysis

Images from HT-qFISH were acquired on an Opera High Content Screening System (PerkinElmer) as in [57], using 40×, 0.9 NA water-immersion objective at the Microscopy Unit of Spanish National Cancer Research Center (CNIO). To ensure that a minimum of 300 cells per case were scored, 40 images were acquired in each well. Images were analyzed with Acapella Software [57]. Images from ovarian sections were acquired on a Confocal TCS SP5 Leica Microscope equipped with a resonant scanner using a 63×, 1.4 NA oil-immersion objective at the Microscopy and Image Analysis Service (SMAI) of the National Hospital for Paraplegics of Toledo, Spain. DAPI and Cy3 signals were acquired on separate channels. Maximum-projection images from Z-stacks were used for quantitative analysis [77]. Quantitative data analysis was performed using Fiji (ImageJ 1.53f51) software with the assistance of the SMAI. For the detection of signals, the background noise of the maximum projections was subtracted. Maximum-projection signals were thresholded, and CY3 signals corresponding to telomeres, were detected with the "Analyze particles" command of ImageJ. DAPI signals were also detected to define the nuclear area, so that only telomere signals from inside the nuclear mask were considered [78]. The detections were saved in the ROI Manager to be transferred to the unprocessed images for intensity quantification. Mean CY3 intensity per telomeric spot was used for quantification and expressed as arbitrary units (a.u.) [78]. Telomeres from global ovarian tissue and GCs were analyzed. Follicle types were classified as described above (see follicle count section). Not all follicular types were present in each ovarian section, thus, the number of samples varied in experiments related to follicular types (Figure 3E–3G and Table 2).

Reproductive outcomes

Middle-aged SAMP8 and SAMR1 females (7-months old) were superovulated by intraperitoneal injection of 10 I.U. of pregnant mare serum gonadotropin (PMSG, Folligon, MSD Animal Health) and 10 I.U. of human chorionic gonadotrophin (hCG, LeonVet) and mated with a fertile-young male. After 1.5 days, females were sacrificed, and oocytes were retrieved from the oviducts and the number of total collected oocytes was measured. Successful fertilization was confirmed by the presence of ≥ 2-cell embryos in maternal reproductive tract. Fertilization rate was calculated as the ratio of embryos divided by the number of oocytes and embryos collected. Preimplantation embryos were collected from the uterus at 3.5 days after mating. Data collection in terms of reproductive outcomes is variable because SAMP8 females do not always respond to OS (Figure 4E–4G).

Statistics

All statistical analysis were performed using GraphPad Prism software (version 8). Data were presented as mean and standard error and the Shapiro-Wilk test was used to determine whether the data followed a normal distribution. Student's *t*-test was applied to compare groups for variables that followed a normal distribution and the two-tailed Mann-Whitney *U* test was applied as a nonparametric method to analyze variables that did not follow a normal distribution. Log-rank test was applied to detect differences between survival curves. Fisher's exact test was used to determine statistical significance for the analysis of probabilities in contingency tables. p values < 0.05 were considered statistically significant. The number of samples used for each experiment is indicated in the figures.

Abbreviations

A.U.: Arbitrary Units; DAPI: 4′,6-Diamidino-2-phenylindole; DNA: Deoxyribonucleic Acid; FISH: Fluorescence *In Situ* Hybridization; GAPDH: Glyceraldehyde-3-phosphate dehydrogenase; GCs: Granulosa Cells; HT q-FISH: High Throughput Quantitative Fluorescence *In Situ* Hybridization; H&E: Hematoxylin–Eosin; OS: Ovarian Stimulation; PBMCs: Peripheral Blood Mononuclear Cells; RNA: Ribonucleic Acid; RT: Room Temperature; RTqPCR: Real-Time Quantitative Polymerase Chain Reaction; SAMP8: Senescence Accelerated Mouse Prone 8; SAMR1: Senescence Accelerated Mouse Resistant 1; SMAI: Microscopy and Image Analysis Service; TA: Telomerase Activity; TERC: Telomerase RNA Component; TERT: Telomerase Reverse Transcriptase Component; TL: Telomere Length; TRAP: Telomerase-repeat amplification protocol.

AUTHOR CONTRIBUTIONS

A.M.P. performed animal handling, collected and processed samples, performed all experiments, analyzed the results, performed statistical analysis, discussed

results and wrote the manuscript. M.M. performed mouse handling, collected samples and provided technical assistance with experiments. L.C-S. provided technical assistance with experiments, discussed results and performed critical reading of the manuscript. I.C-O. helped with animal handling, discussed results and did critical reading of the manuscript. M.C. Performed follicular count, discussed results and made a critical reading of the manuscript. S.H. contributed to experimental design, performed follicular count and made critical reading of the manuscript. E.S. performed follicular count, discussed results and made a critical review of the manuscript. J.M. performed H&E tinctions and performed the anatomopathological analysis on ovarian sections and embryo morphology as well as postmortem examinations. A.P. contributed to experimental design, discussed results and did critical reading of the manuscript. J.A.G-V. obtained funds for the laboratory, contributed to experimental design, discussed results, did critical reading of the manuscript, and E.V. obtained funds for the laboratory, designed experiments, wrote the protocol for CEI approval, supervised experiments, analyzed and discussed results and wrote the manuscript with A.M.P.

ACKNOWLEDGMENTS

The authors would like to thank Jesús Gómez (from CNIO Microscopy Unit) and Javier Mazarío (from SMAI-HNP) for their assistance in image acquisition and analysis.

CONFLICTS OF INTEREST

The authors declare no conflicts of interest related to this study.

ETHICAL STATEMENT

All animal procedures were performed according to protocols approved by the Ethics Committee of the Rey Juan Carlos University (code 2509201913119) on 18th of November of 2019.

FUNDING

This study has been funded by Instituto de Salud Carlos III (ISCIII) through the project PI20/00252 and co-funded by the European Union. The Laboratory of Telomeres and Reproduction is also supported by CDTI and FEDER through IDI-20190160 to J.A.G.V.; by Ferring COVID-19 grant in RM to E.V.; by FINOX through FORWARD 2018_6 to E.V. and J.A.G.V. and by IVIRMA (1711-FIVI-111-MV). E.V. was funded by Spanish Ministry of Science and Innovation through a Torres Quevedo grant (PTQ-16-08242). A.M.P. is supported by the Spanish Ministry of Science, Innovation and Universities (FPU 18/02904). L.C-S. is supported by the Instituto de Salud Carlos III (Spanish Government) through FI19/00008 and European Union (ESF, "Investing in your Future"). I.C-O. is supported by the Spanish Ministry of Science, Innovation and Universities (FPU 18/04068). S.H. participation was funded by the CP19/00141 grant from Instituto de Salud Carlos III and co-funded by European Union (ESF, "Investing in your Future").

REFERENCES

1. Hawkes K. Grandmothers and the evolution of human longevity. Am J Hum Biol. 2003; 15:380–400. https://doi.org/10.1002/ajhb.10156 PMID:12704714

2. Chico-Sordo L, Córdova-Oriz I, Polonio AM, S-Mellado LS, Medrano M, García-Velasco JA, Varela E. Reproductive aging and telomeres: Are women and men equally affected? Mech Ageing Dev. 2021; 198:111541. https://doi.org/10.1016/j.mad.2021.111541 PMID:34245740

3. Polonio AM, Chico-Sordo L, Córdova-Oriz I, Medrano M, García-Velasco JA, Varela E. Impact of Ovarian Aging in Reproduction: From Telomeres and Mice Models to Ovarian Rejuvenation. Yale J Biol Med. 2020; 93:561–9. PMID:33005120

4. Varela E, Sánchez-de-Puerta I, García-Velasco JA. Fertility, IVF and reproductive genetics. Curr Opin Obstet Gynecol. 2018; 30:203–8. https://doi.org/10.1097/GCO.0000000000000456 PMID:29708900

5. Thong EP, Hart RJ, Teede HJ, Vincent AJ, Enticott JC. Increased mortality and non-cancer morbidity risk may be associated with early menopause and varies with aetiology: An exploratory population-based study using data-linkage. Maturitas. 2022; 164:60–6. https://doi.org/10.1016/j.maturitas.2022.06.011 PMID:35803198

6. Agrinier N, Cournot M, Dallongeville J, Arveiler D, Ducimetière P, Ruidavets JB, Ferrières J. Menopause and modifiable coronary heart disease risk factors: a population based study. Maturitas. 2010; 65:237–43. https://doi.org/10.1016/j.maturitas.2009.11.023 PMID:20031345

7. López-Otín C, Blasco MA, Partridge L, Serrano M, Kroemer G. The hallmarks of aging. Cell. 2013; 153:1194–217. https://doi.org/10.1016/j.cell.2013.05.039 PMID:23746838

8. Blackburn EH. Structure and function of telomeres. Nature. 1991; 350:569–73. https://doi.org/10.1038/350569a0 PMID:1708110

9. Olovnikov AM. A theory of marginotomy. The incomplete copying of template margin in enzymic synthesis of polynucleotides and biological significance of the phenomenon. J Theor Biol. 1973; 41:181–90. https://doi.org/10.1016/0022-5193(73)90198-7 PMID:4754905

10. Hemann MT, Strong MA, Hao LY, Greider CW. The shortest telomere, not average telomere length, is critical for cell viability and chromosome stability. Cell. 2001; 107:67–77. https://doi.org/10.1016/s0092-8674(01)00504-9 PMID:11595186

11. Kaul Z, Cesare AJ, Huschtscha LI, Neumann AA, Reddel RR. Five dysfunctional telomeres predict onset of senescence in human cells. EMBO Rep. 2011; 13:52–9. https://doi.org/10.1038/embor.2011.227 PMID:22157895

12. Donate LE, Blasco MA. Telomeres in cancer and ageing. Philos Trans R Soc Lond B Biol Sci. 2011; 366:76–84. https://doi.org/10.1098/rstb.2010.0291 PMID:21115533

13. Takubo K, Nakamura K, Izumiyama N, Furugori E, Sawabe M, Arai T, Esaki Y, Mafune K, Kammori M, Fujiwara M, Kato M, Oshimura M, Sasajima K. Telomere shortening with aging in human liver. J Gerontol A Biol Sci Med Sci. 2000; 55:B533–6. https://doi.org/10.1093/gerona/55.11.b533 PMID:11078086

14. Armanios M. The Role of Telomeres in Human Disease. Annu Rev Genomics Hum Genet. 2022; 23:363–81. https://doi.org/10.1146/annurev-genom-010422-091101 PMID:35609925

15. Martínez P, Blasco MA. Telomere-driven diseases and telomere-targeting therapies. J Cell Biol. 2017; 216:875–87. https://doi.org/10.1083/jcb.201610111 PMID:28254828

16. Cawthon RM, Smith KR, O'Brien E, Sivatchenko A, Kerber RA. Association between telomere length in blood and mortality in people aged 60 years or older. Lancet. 2003; 361:393–5. https://doi.org/10.1016/S0140-6736(03)12384-7 PMID:12573379

17. Greider CW, Blackburn EH. The telomere terminal transferase of Tetrahymena is a ribonucleoprotein enzyme with two kinds of primer specificity. Cell. 1987; 51:887–98. https://doi.org/10.1016/0092-8674(87)90576-9 PMID:3319189

18. Flores I, Cayuela ML, Blasco MA. Effects of telomerase and telomere length on epidermal stem cell behavior. Science. 2005; 309:1253–6. https://doi.org/10.1126/science.1115025 PMID:16037417

19. Lee HW, Blasco MA, Gottlieb GJ, Horner JW 2nd, Greider CW, DePinho RA. Essential role of mouse telomerase in highly proliferative organs. Nature. 1998; 392:569–74. https://doi.org/10.1038/33345 PMID:9560153

20. Hao LY, Armanios M, Strong MA, Karim B, Feldser DM, Huso D, Greider CW. Short telomeres, even in the presence of telomerase, limit tissue renewal capacity. Cell. 2005; 123:1121–31. https://doi.org/10.1016/j.cell.2005.11.020 PMID:16360040

21. Herrera E, Samper E, Martín-Caballero J, Flores JM, Lee HW, Blasco MA. Disease states associated with telomerase deficiency appear earlier in mice with short telomeres. EMBO J. 1999; 18:2950–60. https://doi.org/10.1093/emboj/18.11.2950 PMID:10357808

22. Rudolph KL, Chang S, Lee HW, Blasco M, Gottlieb GJ, Greider C, DePinho RA. Longevity, stress response, and cancer in aging telomerase-deficient mice. Cell. 1999; 96:701–12. https://doi.org/10.1016/s0092-8674(00)80580-2 PMID:10089885

23. García-Cao I, García-Cao M, Tomás-Loba A, Martín-Caballero J, Flores JM, Klatt P, Blasco MA, Serrano M. Increased p53 activity does not accelerate telomere-driven ageing. EMBO Rep. 2006; 7:546–52. https://doi.org/10.1038/sj.embor.7400667 PMID:16582880

24. Blasco MA, Lee HW, Hande MP, Samper E, Lansdorp PM, DePinho RA, Greider CW. Telomere shortening and tumor formation by mouse cells lacking telomerase RNA. Cell. 1997; 91:25–34. https://doi.org/10.1016/s0092-8674(01)80006-4 PMID:9335332

25. Vulliamy TJ, Marrone A, Knight SW, Walne A, Mason PJ, Dokal I. Mutations in dyskeratosis congenita: their impact on telomere length and the diversity of clinical presentation. Blood. 2006; 107:2680–5. https://doi.org/10.1182/blood-2005-07-2622 PMID:16332973

26. Vulliamy T, Marrone A, Goldman F, Dearlove A, Bessler M, Mason PJ, Dokal I. The RNA component of telomerase is mutated in autosomal dominant dyskeratosis congenita. Nature. 2001; 413:432–5. https://doi.org/10.1038/35096585 PMID:11574891

27. Vulliamy T, Marrone A, Dokal I, Mason PJ. Association between aplastic anaemia and mutations in telomerase RNA. Lancet. 2002; 359:2168–70. https://doi.org/10.1016/S0140-6736(02)09087-6 PMID:12090986

28. Gaysinskaya V, Stanley SE, Adam S, Armanios M. Synonymous Mutation in DKC1 Causes Telomerase RNA Insufficiency Manifesting as Familial Pulmonary Fibrosis. Chest. 2020; 158:2449–57. https://doi.org/10.1016/j.chest.2020.07.025 PMID:32710892

29. Wright WE, Piatyszek MA, Rainey WE, Byrd W, Shay JW. Telomerase activity in human germline and embryonic tissues and cells. Dev Genet. 1996; 18:173–9. https://doi.org/10.1002/(SICI)1520-6408(1996)18:2<173::AID-DVG10>3.0.CO;2-3 PMID:8934879

30. Mantell LL, Greider CW. Telomerase activity in germline and embryonic cells of Xenopus. EMBO J. 1994; 13:3211–7. https://doi.org/10.1002/j.1460-2075.1994.tb06620.x PMID:8039513

31. Betts DH, King WA. Telomerase activity and telomere detection during early bovine development. Dev Genet. 1999; 25:397–403. https://doi.org/10.1002/(SICI)1520-6408(1999)25:4<397::AID-DVG13>3.0.CO;2-J PMID:10570471

32. Liu L, Bailey SM, Okuka M, Muñoz P, Li C, Zhou L, Wu C, Czerwiec E, Sandler L, Seyfang A, Blasco MA, Keefe DL. Telomere lengthening early in development. Nat Cell Biol. 2007; 9:1436–41. https://doi.org/10.1038/ncb1664 PMID:17982445

33. Wang W, Chen H, Li R, Ouyang N, Chen J, Huang L, Mai M, Zhang N, Zhang Q, Yang D. Telomerase activity is more significant for predicting the outcome of IVF treatment than telomere length in granulosa cells. Reproduction. 2014; 147:649–57. https://doi.org/10.1530/REP-13-0223 PMID:24472817

34. Yamagata Y, Nakamura Y, Umayahara K, Harada A, Takayama H, Sugino N, Kato H. Changes in telomerase activity in experimentally induced atretic follicles of immature rats. Endocr J. 2002; 49:589–95. https://doi.org/10.1507/endocrj.49.589 PMID:12625407

35. Pedroso DCC, Santana VP, Donaires FS, Picinato MC, Giorgenon RC, Santana BA, Pimentel RN, Keefe DL, Calado RT, Ferriani RA, Furtado CLM, Reis RM. Telomere Length and Telomerase Activity in Immature Oocytes and Cumulus Cells of Women with Polycystic Ovary Syndrome. Reprod Sci. 2020; 27:1293–303. https://doi.org/10.1007/s43032-019-00120-6 PMID:32046456

36. Córdova-Oriz I, Chico-Sordo L, Varela E. Telomeres, aging and reproduction. Curr Opin Obstet Gynecol. 2022; 34:151–8. https://doi.org/10.1097/GCO.0000000000000779 PMID:35645014

37. Treff NR, Su J, Taylor D, Scott RT Jr. Telomere DNA deficiency is associated with development of human embryonic aneuploidy. PLoS Genet. 2011; 7:e1002161. https://doi.org/10.1371/journal.pgen.1002161 PMID:21738493

38. Butts S, Riethman H, Ratcliffe S, Shaunik A, Coutifaris C, Barnhart K. Correlation of telomere length and telomerase activity with occult ovarian insufficiency. J Clin Endocrinol Metab. 2009; 94:4835–43. https://doi.org/10.1210/jc.2008-2269 PMID:19864453

39. Hanna CW, Bretherick KL, Gair JL, Fluker MR, Stephenson MD, Robinson WP. Telomere length and reproductive aging. Hum Reprod. 2009; 24:1206–11. https://doi.org/10.1093/humrep/dep007 PMID:19202142

40. Xu X, Chen X, Zhang X, Liu Y, Wang Z, Wang P, Du Y, Qin Y, Chen ZJ. Impaired telomere length and telomerase activity in peripheral blood leukocytes and granulosa cells in patients with biochemical primary ovarian insufficiency. Hum Reprod. 2017; 32:201–7. https://doi.org/10.1093/humrep/dew283 PMID:27836977

41. Miranda-Furtado CL, Luchiari HR, Chielli Pedroso DC, Kogure GS, Caetano LC, Santana BA, Santana VP, Benetti-Pinto CL, Reis FM, Maciel MA, Ferriani RA, Ramos ES, Calado RT, Dos Reis RM. Skewed X-chromosome inactivation and shorter telomeres associate with idiopathic premature ovarian insufficiency. Fertil Steril. 2018; 110:476–85.e1. https://doi.org/10.1016/j.fertnstert.2018.04.017 PMID:30098699

42. Takeda T. Senescence-accelerated mouse (SAM) with special references to neurodegeneration models,

SAMP8 and SAMP10 mice. Neurochem Res. 2009; 34:639–59.
https://doi.org/10.1007/s11064-009-9922-y
PMID:19199030

43. Bernstein LR, Mackenzie AC, Kraemer DC, Morley JE, Farr S, Chaffin CL, Merchenthaler I. Shortened estrous cycle length, increased FSH levels, FSH variance, oocyte spindle aberrations, and early declining fertility in aging senescence-accelerated mouse prone-8 (SAMP8) mice: concomitant characteristics of human midlife female reproductive aging. Endocrinology. 2014; 155:2287–300.
https://doi.org/10.1210/en.2013-2153
PMID:24654787

44. Takeda T, Hosokawa M, Higuchi K. Senescence-accelerated mouse (SAM): a novel murine model of senescence. Exp Gerontol. 1997; 32:105–9.
https://doi.org/10.1016/s0531-5565(96)00036-8
PMID:9088907

45. Takeda T, Hosokawa M, Higuchi K, Hosono M, Akiguchi I, Katoh H. A novel murine model of aging, Senescence-Accelerated Mouse (SAM). Arch Gerontol Geriatr. 1994; 19:185–92.
https://doi.org/10.1016/0167-4943(94)90039-6
PMID:15374284

46. Powers DC, Morley JE, Flood JF. Age-related changes in LFA-1 expression, cell adhesion, and PHA-induced proliferation by lymphocytes from senescence-accelerated mouse (SAM)-P/8 and SAM-R/1 substrains. Cell Immunol. 1992; 141:444–56.
https://doi.org/10.1016/0008-8749(92)90162-i
PMID:1576658

47. Pang KC, Miller JP, Fortress A, McAuley JD. Age-related disruptions of circadian rhythm and memory in the senescence-accelerated mouse (SAMP8). Age (Dordr). 2006; 28:283–96.
https://doi.org/10.1007/s11357-006-9013-9
PMID:22253495

48. Miyamoto M. Characteristics of age-related behavioral changes in senescence-accelerated mouse SAMP8 and SAMP10. Exp Gerontol. 1997; 32:139–48.
https://doi.org/10.1016/s0531-5565(96)00061-7
PMID:9088911

49. Morley JE. The SAMP8 mouse: a model of Alzheimer disease? Biogerontology. 2002; 3:57–60.
https://doi.org/10.1023/a:1015207429786
PMID:12014843

50. Takeda T. Senescence-accelerated mouse (SAM): a biogerontological resource in aging research. Neurobiol Aging. 1999; 20:105–10.
https://doi.org/10.1016/s0197-4580(99)00008-1
PMID:10537019

51. Flood JF, Farr SA, Kaiser FE, La Regina M, Morley JE. Age-related decrease of plasma testosterone in SAMP8 mice: replacement improves age-related impairment of learning and memory. Physiol Behav. 1995; 57:669–73.
https://doi.org/10.1016/0031-9384(94)00318-1
PMID:7777601

52. Carter TA, Greenhall JA, Yoshida S, Fuchs S, Helton R, Swaroop A, Lockhart DJ, Barlow C. Mechanisms of aging in senescence-accelerated mice. Genome Biol. 2005; 6:R48.
https://doi.org/10.1186/gb-2005-6-6-r48
PMID:15960800

53. Wang J, Cheng K, Qin Z, Wang Y, Zhai L, You M, Wu J. Effects of electroacupuncture at Guanyuan (CV 4) or Sanyinjiao (SP 6) on hypothalamus-pituitary-ovary axis and spatial learning and memory in female SAMP8 mice. J Tradit Chin Med. 2017; 37:96–100.
https://doi.org/10.1016/s0254-6272(17)30032-8
PMID:29957916

54. Yuan M, Wen-Xia Z, Jun-Ping C, Yong-Xiang Z. Age-related changes in the oestrous cycle and reproductive hormones in senescence-accelerated mouse. Reprod Fertil Dev. 2005; 17:507–12.
https://doi.org/10.1071/rd04099
PMID:15907275

55. Liu L, Blasco MA, Keefe DL. Requirement of functional telomeres for metaphase chromosome alignments and integrity of meiotic spindles. EMBO Rep. 2002; 3:230–4.
https://doi.org/10.1093/embo-reports/kvf055
PMID:11882542

56. Liu L, Blasco M, Trimarchi J, Keefe D. An essential role for functional telomeres in mouse germ cells during fertilization and early development. Dev Biol. 2002; 249:74–84.
https://doi.org/10.1006/dbio.2002.0735
PMID:12217319

57. Vera E, Bernardes de Jesus B, Foronda M, Flores JM, Blasco MA. The rate of increase of short telomeres predicts longevity in mammals. Cell Rep. 2012; 2:732–7.
https://doi.org/10.1016/j.celrep.2012.08.023
PMID:23022483

58. Nakamura TM, Morin GB, Chapman KB, Weinrich SL, Andrews WH, Lingner J, Harley CB, Cech TR. Telomerase catalytic subunit homologs from fission yeast and human. Science. 1997; 277:955–9.
https://doi.org/10.1126/science.277.5328.955
PMID:9252327

59. Takeda T, Matsushita T, Kurozumi M, Takemura K, Higuchi K, Hosokawa M. Pathobiology of the

senescence-accelerated mouse (SAM). Exp Gerontol. 1997; 32:117–27.
https://doi.org/10.1016/s0531-5565(96)00068-x
PMID:9088909

60. Ye X, Meeker HC, Kozlowski PB, Wegiel J, Wang KC, Imaki H, Carp RI. Pathological changes in the liver of a senescence accelerated mouse strain (SAMP8): a mouse model for the study of liver diseases. Histol Histopathol. 2004; 19:1141–51.
https://doi.org/10.14670/HH-19.1141
PMID:15375757

61. Muñoz-Espín D, Serrano M. Cellular senescence: from physiology to pathology. Nat Rev Mol Cell Biol. 2014; 15:482–96.
https://doi.org/10.1038/nrm3823
PMID:24954210

62. Serrano M, Barzilai N. Targeting senescence. Nat Med. 2018; 24:1092–4.
https://doi.org/10.1038/s41591-018-0141-4
PMID:30082861

63. Greider CW, Blackburn EH. Identification of a specific telomere terminal transferase activity in Tetrahymena extracts. Cell. 1985; 43:405–13.
https://doi.org/10.1016/0092-8674(85)90170-9
PMID:3907856

64. Carvalho VS, Gomes WR, Calado RT. Recent advances in understanding telomere diseases. Fac Rev. 2022; 11:31.
https://doi.org/10.12703/r/11-31
PMID:36311538

65. Alder JK, Parry EM, Yegnasubramanian S, Wagner CL, Lieblich LM, Auerbach R, Auerbach AD, Wheelan SJ, Armanios M. Telomere phenotypes in females with heterozygous mutations in the dyskeratosis congenita 1 (DKC1) gene. Hum Mutat. 2013; 34:1481–5.
https://doi.org/10.1002/humu.22397
PMID:23946118

66. Robinson LG Jr, Pimentel R, Wang F, Kramer YG, Gonullu DC, Agarwal S, Navarro PA, McCulloh D, Keefe DL. Impaired reproductive function and fertility preservation in a woman with a dyskeratosis congenita. J Assist Reprod Genet. 2020; 37:1221–5.
https://doi.org/10.1007/s10815-020-01758-x
PMID:32405899

67. Vaskivuo TE, Ottander U, Oduwole O, Isomaa V, Vihko P, Olofsson JI, Tapanainen JS. Role of apoptosis, apoptosis-related factors and 17beta-hydroxysteroid dehydrogenases in human corpus luteum regression. Mol Cell Endocrinol. 2002; 194:191–200.
https://doi.org/10.1016/s0303-7207(02)00087-4
PMID:12242042

68. Rolaki A, Drakakis P, Millingos S, Loutradis D, Makrigiannakis A. Novel trends in follicular development, atresia and corpus luteum regression: a role for apoptosis. Reprod Biomed Online. 2005; 11:93–103.
https://doi.org/10.1016/s1472-6483(10)61304-1
PMID:16102296

69. Franasiak JM, Forman EJ, Hong KH, Werner MD, Upham KM, Treff NR, Scott RT Jr. The nature of aneuploidy with increasing age of the female partner: a review of 15,169 consecutive trophectoderm biopsies evaluated with comprehensive chromosomal screening. Fertil Steril. 2014; 101:656–63.e1.
https://doi.org/10.1016/j.fertnstert.2013.11.004
PMID:24355045

70. Prescott JC, Blackburn EH. Telomerase RNA template mutations reveal sequence-specific requirements for the activation and repression of telomerase action at telomeres. Mol Cell Biol. 2000; 20:2941–8.
https://doi.org/10.1128/MCB.20.8.2941-2948.2000
PMID:10733598

71. Russo V, Berardinelli P, Martelli A, Di Giacinto O, Nardinocchi D, Fantasia D, Barboni B. Expression of telomerase reverse transcriptase subunit (TERT) and telomere sizing in pig ovarian follicles. J Histochem Cytochem. 2006; 54:443–55.
https://doi.org/10.1369/jhc.4A6603.2006
PMID:16400001

72. Gaytan F, Morales C, Bellido C, Aguilar E, Sanchez-Criado JE. Proliferative activity in the different ovarian compartments in cycling rats estimated by the 5-bromodeoxyuridine technique. Biol Reprod. 1996; 54:1356–65.
https://doi.org/10.1095/biolreprod54.6.1356
PMID:8724365

73. Novella-Maestre E, Herraiz S, Rodríguez-Iglesias B, Díaz-García C, Pellicer A. Short-Term PTEN Inhibition Improves In Vitro Activation of Primordial Follicles, Preserves Follicular Viability, and Restores AMH Levels in Cryopreserved Ovarian Tissue From Cancer Patients. PLoS One. 2015; 10:e0127786.
https://doi.org/10.1371/journal.pone.0127786
PMID:26024525

74. García-Cao M, Gonzalo S, Dean D, Blasco MA. A role for the Rb family of proteins in controlling telomere length. Nat Genet. 2002; 32:415–9.
https://doi.org/10.1038/ng1011
PMID:12379853

75. Mender I, Shay JW. Telomerase Repeated Amplification Protocol (TRAP). Bio Protoc. 2015; 5:e1657.
https://doi.org/10.21769/bioprotoc.1657
PMID:27182535

76. Varela E, Muñoz-Lorente MA, Tejera AM, Ortega S, Blasco MA. Generation of mice with longer and better

preserved telomeres in the absence of genetic manipulations. Nat Commun. 2016; 7:11739. https://doi.org/10.1038/ncomms11739 PMID:27252083

77. Flores I, Canela A, Vera E, Tejera A, Cotsarelis G, Blasco MA. The longest telomeres: a general signature of adult stem cell compartments. Genes Dev. 2008; 22:654–67. https://doi.org/10.1101/gad.451008 PMID:18283121

78. Schneider RP, Garrobo I, Foronda M, Palacios JA, Marión RM, Flores I, Ortega S, Blasco MA. TRF1 is a stem cell marker and is essential for the generation of induced pluripotent stem cells. Nat Commun. 2013; 4:1946. https://doi.org/10.1038/ncomms2946 PMID:23735977

SUPPLEMENTARY MATERIALS

Supplementary Figures

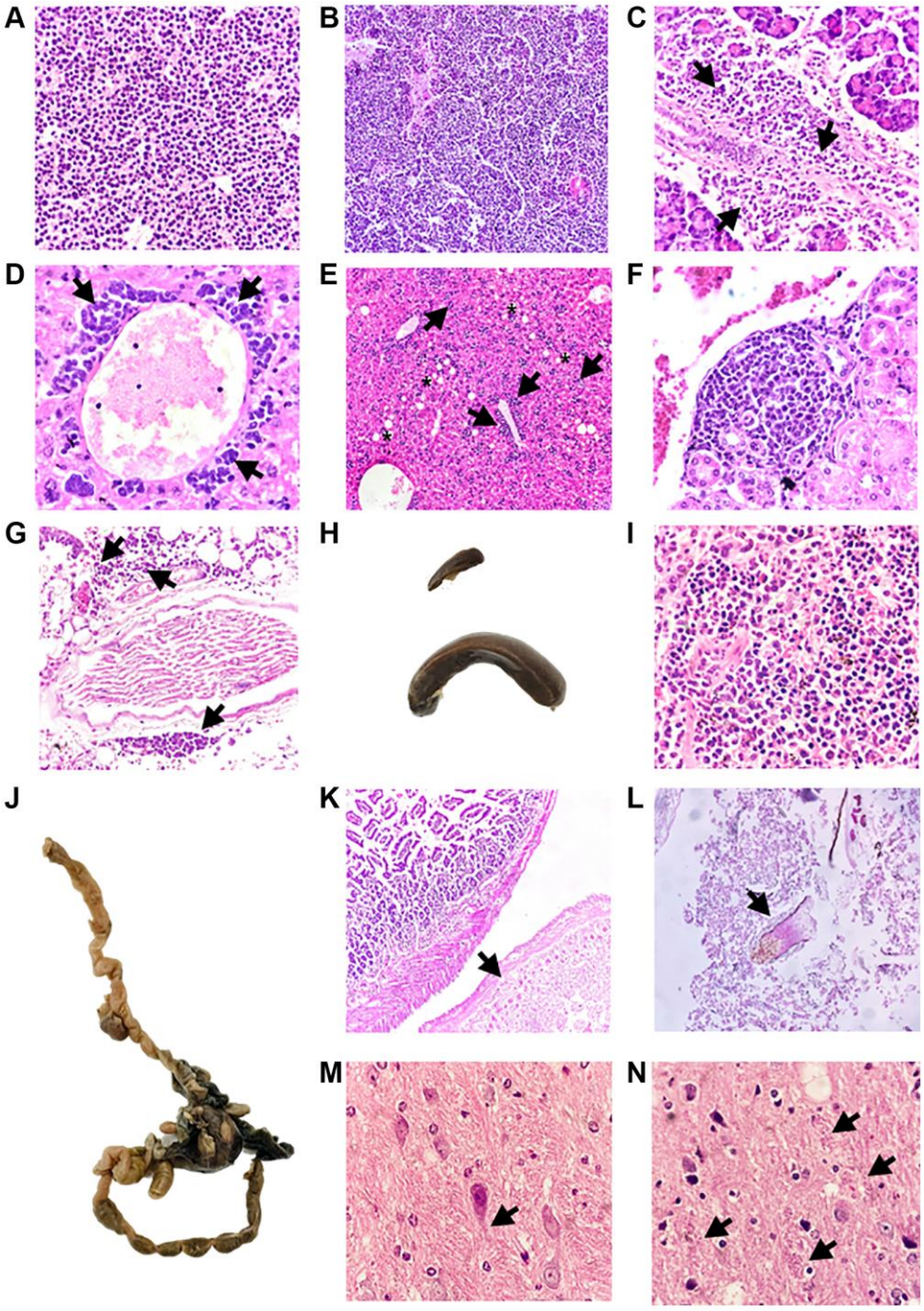

Supplementary Figure 1. Postmortem examinations of SAMP8 mice. Representative micrographs of necropsies in SAMP8. (**A**) Diffuse tumor infiltration of the thymus by lymphoid cells (SAMP8-18). (**B**) Lymphoid tumor with diffuse growth of cells of plasmablastic habitus in lymph node (SAMP8-07). (**C**) Lymphoid tumor lesions (indicated with arrows) in pancreatic tissue (SAMP8-07). (**D**) Lymphoid neoplasm infiltration (arrows) in hepatic perivenular areas (SAMP8-04). (**E**) Lymphoid tumor cellularity (plasmablastic, indicated with arrows) in hepatic sinusoids and perivenular areas (SAMP8-04). Asterisks indicate the presence of lipid droplets reflecting hepatic steatosis. (**F**) Lymphoid tumor lesions in kidney and (**G**) perirenal tissue (SAMP8-04). (**H**) Splenomegaly found in SAMP8 mice (SAMP8-07) (bottom) compared with a control spleen (top). (**I**) Diffuse splenic infiltration of lymphoma (SAMP8-18). (**J**) Intestinal torsion and necrosis (SAMP8-07). (**K**) Ischemic lesion (arrows) and (**L**) hairs (indicated with arrow) in feces in the intestine described in J. (**M**) Neurofibrillary tangles (indicated with arrows) in the brain (SAMPB-21). (**N**) Possible amyloid plaques (indicated with arrows) in brain (SAMP8-25).

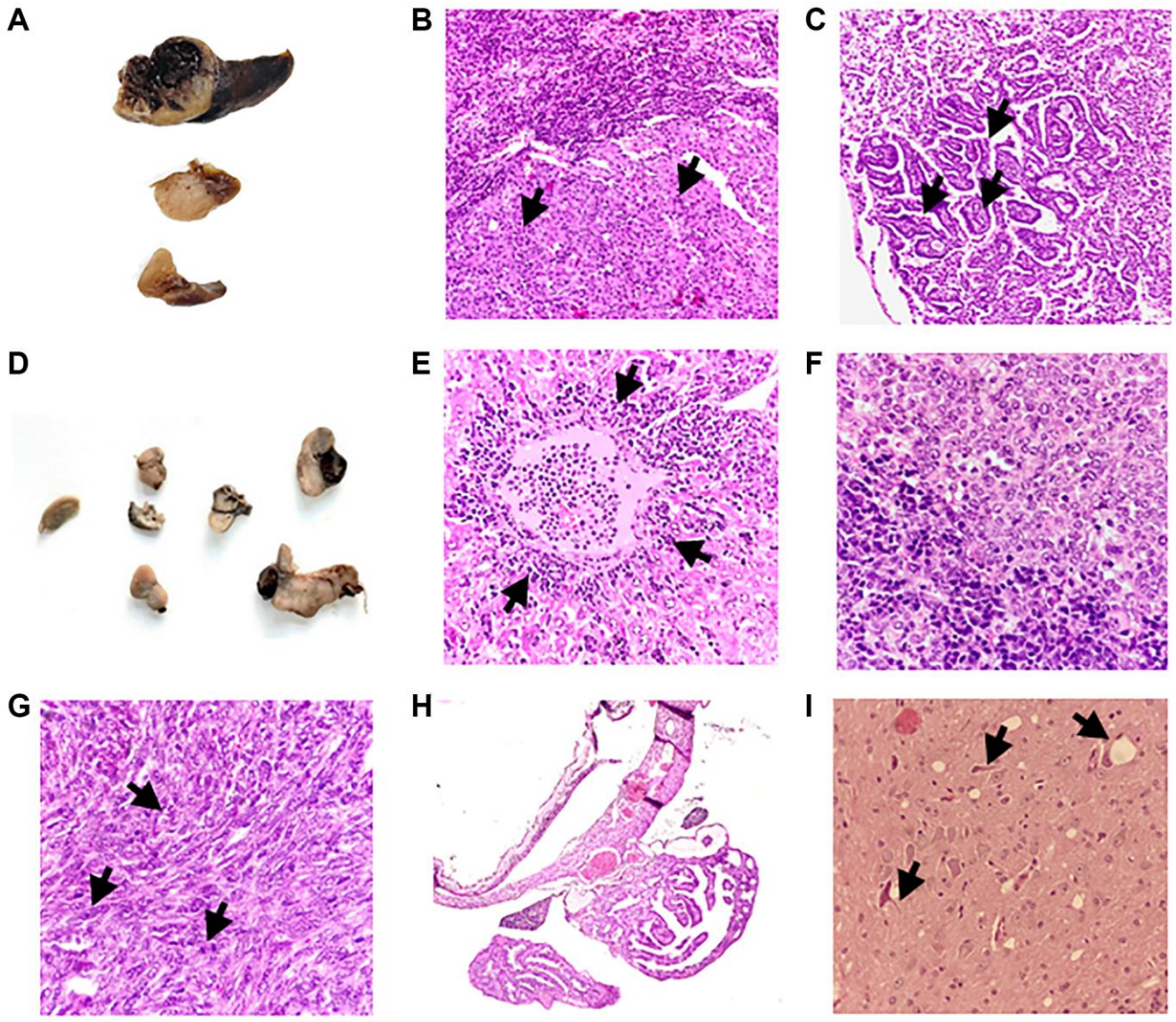

Supplementary Figure 2. Postmortem examinations of SAMR1 mice. Representative micrographs of necropsies in SAMR1. (**A**) Macroscopic image of a lung tumor (SAMR1-37). (**B**, **C**) Tumor foci in the lung consisting of papillary adenocarcinomas (SAMR1-37 in B and SAMR1-14 in C). Arrows indicate tumor areas. (**D**) Macroscopic image of lymph nodes thickened by tumors located adjacent to the colon, kidney and cervical region (SAMR1-07). (**E**) Metastasis of the lymphoma described in D in perivenular areas of liver, in the form of a small and large cell lymphoma (indicated by arrows). (**F**) Metastasis of the lymphoma described in D, infiltrated in spleen. Different cell morphologies are found. (**G**) Sarcoma in the abdominal wall (SAMR1 -25) consisting of a malignant spindle-cell lesion. Arrows indicate mitotic figures. (**H**) Image shows a benign cyst in peritoneum (SAMR1 -13). (**I**) Neurofibrillary tangles (indicated with arrows) in the brain (SAMR1 -25).

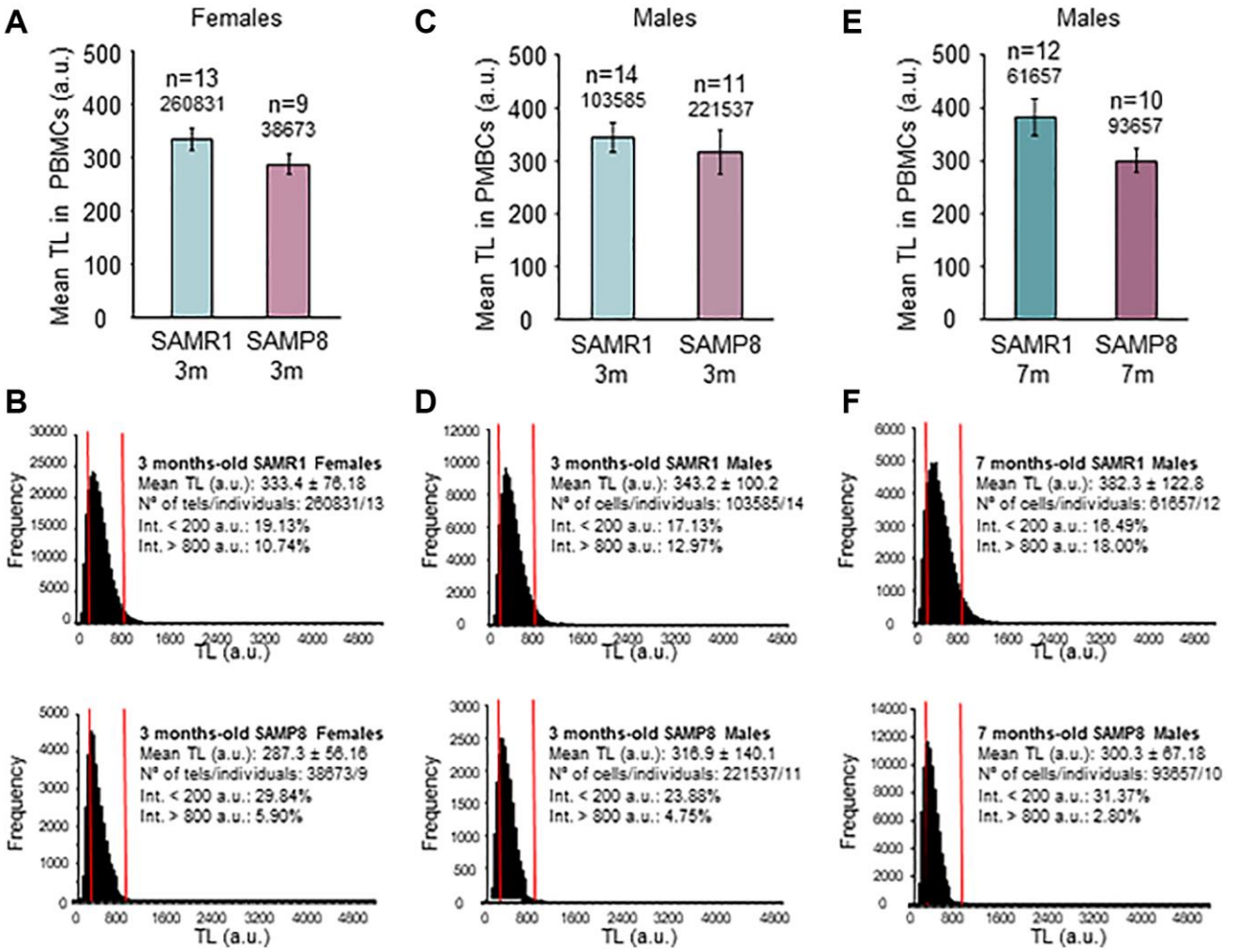

Supplementary Figure 3. Analysis of telomere length in PBMCs. (**A**) Mean TL of PBMCs, analyzed by HT-qFISH, in 3-month-old SAMP8 and SAMR1 females. (**B**) Telomere-length frequency histograms in 3-month-old SAMR1 (top panel) and SAMP8 females (lower panel). (**C**) Mean TL of PBMCs, analyzed by HT-qFISH, in 3-month-old SAMP8 and SAMR1 males. (**D**) Telomere-length frequency histograms in 3-month-old SAMR1 (top panel) and SAMP8 males (lower panel). (**E**) Mean TL of PBMCs, analyzed by HT-qFISH, in 7-month-old SAMP8 and SAMR1 males. (**F**) Telomere-length frequency histograms in 7-month-old SAMR1 (top panel) and SAMP8 males (lower panel). n indicates the number of mice analyzed. Underneath, the number of telomere spots analyzed is indicated. The S.E.M. is represented in error bars (**A**, **C** and **E**). Statistical significance was determined by unpaired *t*-test (**A**, **C** and **E**). *p*-values < 0.05 were considered statistically significant.

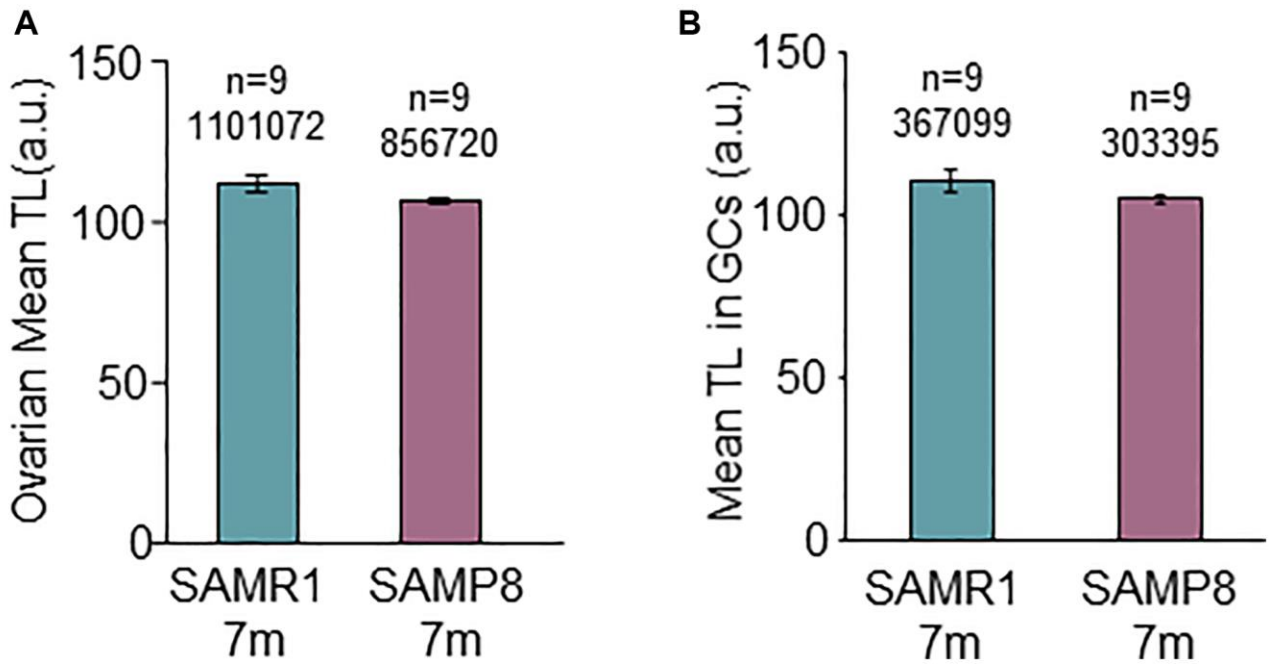

Supplementary Figure 4. Analysis of mean telomere length in the ovary. (**A**) Global mean TL in the ovary of 7-month-old SAMP8 and SAMR1 females, analyzed by FISH. (**B**) Mean TL in GCs of the ovary of mice described in A. n indicates the number of mice analyzed. Underneath, the number of telomere spots analyzed is indicated. The S.E.M. is represented in error bars, Statistical significance was determined by unpaired *t*-test (**B**) and Mann-Whitney *U* test (**A**). *p*-values < 0.05 were considered statistically significant.

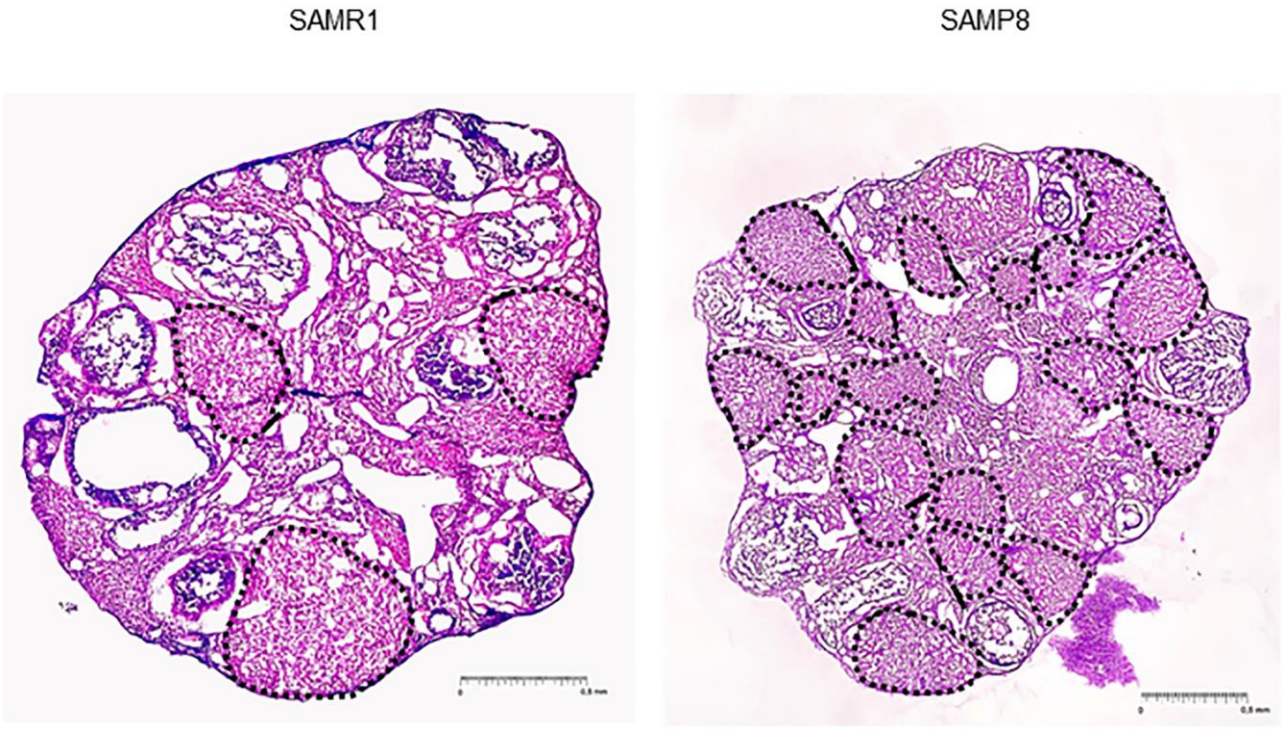

Supplementary Figure 5. Corpus luteum in ovaries. Representative image of ovarian sections from SAMP8 (right panel) and SAMR1 (left panel) females. Dashed lines indicate corpus luteum.

Supplementary Tables

Supplementary Table 1. Individual survival in SAMP8 and SAMR1 mice.

Mice code	Model	Sex	Age at death (weeks)
SAMP8-01	SAMP8	Female	35.57
SAMP8-02	SAMP8	Female	37
SAMP8-03	SAMP8	Female	37.86
SAMP8-04	SAMP8	Female	43.71
SAMP8-05	SAMP8	Male	51
SAMP8-06	SAMP8	Male	32.14
SAMP8-07	SAMP8	Male	61.71
SAMP8-08	SAMP8	Female	59.86
SAMP8-09	SAMP8	Female	96
SAMP8-10	SAMP8	Female	78
SAMP8-11	SAMP8	Female	73
SAMP8-12	SAMP8	Female	60
SAMP8-13	SAMP8	Female	60
SAMP8-14	SAMP8	Female	64.14
SAMP8-15	SAMP8	Female	57.86
SAMP8-16	SAMP8	Female	51.14
SAMP8-17	SAMP8	Female	76
SAMP8-18	SAMP8	Female	81.14
SAMP8-19	SAMP8	Female	57.14
SAMP8-20	SAMP8	Female	55.71
SAMP8-21	SAMP8	Female	78.71
SAMP8-22	SAMP8	Male	88.86
SAMP8-23	SAMP8	Male	71.14
SAMP8-24	SAMP8	Male	88.86
SAMP8-25	SAMP8	Male	97.86
SAMP8-26	SAMP8	Male	89
SAMP8-27	SAMP8	Male	83
SAMP8-28	SAMP8	Male	46
SAMP8-29	SAMP8	Male	79.14
SAMP8-30	SAMP8	Male	73.71
SAMP8-31	SAMP8	Male	73.71
SAMP8-32	SAMP8	Male	83
SAMP8-33	SAMP8	Male	102
SAMP8-34	SAMP8	Male	79.86
SAMP8-35	SAMP8	Male	85
SAMP8-36	SAMP8	Male	75.14
SAMP8-37	SAMP8	Male	59.14
SAMP8-38	SAMP8	Female	78.29

SAMR1-01	SAMR1	Female	17.86
SAMR1-02	SAMR1	Male	43.57
SAMR1-03	SAMR1	Female	52
SAMR1-04	SAMR1	Female	99.86
SAMR1-05	SAMR1	Female	119.29
SAMR1-06	SAMR1	Female	102.43
SAMR1-07	SAMR1	Female	100.71
SAMR1-08	SAMR1	Female	109.71
SAMR1-09	SAMR1	Female	116.57
SAMR1-10	SAMR1	Female	92.71
SAMR1-11	SAMR1	Female	92.29
SAMR1-12	SAMR1	Female	87.71
SAMR1-13	SAMR1	Female	83.71
SAMR1-14	SAMR1	Female	130.43
SAMR1-15	SAMR1	Female	100
SAMR1-16	SAMR1	Female	93
SAMR1-17	SAMR1	Female	79
SAMR1-18	SAMR1	Female	95.14
SAMR1-19	SAMR1	Female	98.14
SAMR1-20	SAMR1	Female	133.14
SAMR1-21	SAMR1	Male	112.29
SAMR1-22	SAMR1	Male	125.71
SAMR1-23	SAMR1	Male	109.86
SAMR1-24	SAMR1	Male	143.14
SAMR1-25	SAMR1	Male	108.71
SAMR1-26	SAMR1	Male	133.14
SAMR1-27	SAMR1	Male	143.86
SAMR1-28	SAMR1	Male	134
SAMR1-29	SAMR1	Male	116.14
SAMR1-30	SAMR1	Male	101.14
SAMR1-31	SAMR1	Male	122.86
SAMR1-32	SAMR1	Male	136.86
SAMR1-33	SAMR1	Male	143.86
SAMR1-34	SAMR1	Male	115
SAMR1-35	SAMR1	Male	106.43
SAMR1-36	SAMR1	Male	105.86
SAMR1-37	SAMR1	Male	101

Supplementary Table 2. Autopsy findings in SAMP8 and SAMR1 mice.

	SAMP8	SAMR1
Probable causes of death	Unknown	Unknown
	Lymphoma	Lung tumor
	Intestinal necrosis and torsion	Ischemia
	Bronchitis and pleuritic	Lymphoma
Postmortem histopathological findings	Lymphoma and leukemia with infiltration in thymus, liver, spleen, pleura, kidney, lymph nodes and perirenal fat.	Benign cyst in peritoneum
	Steatosis in liver.	Papillary adenocarcinoma in lung
	Intestinal abscesses.	Benign tumor in cecum
	Intestinal torsion and necrosis.	Abscess in colon
	Remains of hair in the intestine. Splenomegaly.	Sarcoma
	Thymus thickened by tumor or reactive process.	Ulcer
	Brain with little mass.	Infiltration of lymphoid tumor in liver, spleen, cervical area, lymph nodes and colon
	Neurofibrillary tangles and amyloid plaques in the brain.	Neurofibrillary tangles in brain.